Physics – Uspekhi **53** (10) 971 – 993 (2010)

REVIEWS OF TOPICAL PROBLEMS PACS numbers: 61.05.fg, **61.46.–w**, 75.50.Mm

Small-angle neutron scattering in structure research of magnetic fluids

M V Avdeev, V L Aksenov

DOI: 10.3367/UFNe.0180.201010a.1009

Contents

1. **Introduction** **971**
2. **Subject and method of research** **973**
   2.1 Main types of magnetic fluids; 2.2 Principles of small-angle scattering; 2.3 Peculiarities of small-angle neutron scattering on magnetic nanoparticles
3. **Contrast variation in the scattering by polydisperse superparamagnetic systems** **978**
   3.1 The classical approach for monodisperse nonmagnetic systems; 3.2 Taking polydispersity into account; 3.3 Taking magnetic scattering into account and the contrast variation in magnetic fluids
4. **The structure of nonmagnetized magnetic fluids** **981**
   4.1 Weakly interacting particles; 4.2 Interacting particles; 4.3 Cluster formation
5. **Magnetic fluids in an external magnetic field** **987**
6. **Conclusion** **990**
   References **991**

Abstract. A magnetic fluid (MF) is a liquid dispersion of magnetic nanoparticles coated by surfactants for stabilization. The MF research reviewed in this paper is primarily aimed at investigating the atomic and magnetic structure of MF particles and the way they interact under various conditions by means of small-angle neutron scattering (SANS). The presence of a liquid carrier in the structure and the magnetic properties of MFs, which are very close to those of an ideal superparamagnetic system, allow the effective use of the major neutron scattering features: the strong effect of hydrogen–deuterium isotopic substitution and magnetic scattering. An extension of the contrast variation technique to the structure research on polydisperse and superparamagnetic systems is proposed. The cases of noninteracting and interacting particles, the latter with cluster formation taken into account, are considered for nonmagnetized and magnetized MFs. The polarized neutron scattering analysis of the structure of magnetized MFs is illustrated by examples. Topical problems in further developing the method to study multiparameter systems are identified.

M V Avdeev Frank Laboratory of Neutron Physics,
Joint Institute for Nuclear Research,
ul. Zholio-Kyuri 6, 141980 Dubna, Moscow region, Russian Federation
Tel. (7-49621) 6 26 74. Fax (7-49621) 6 54 84
E-mail: avd@nf.jinr.ru
V L Aksenov Russian Research Center 'Kurchatov Institute,'
pl. Akademika Kurchatova 1, 123182 Moscow, Russian Federation
Tel. (7-499) 196 97 69. Fax (7-499) 196 64 53
E-mail: aksenov@kiae.ru

Received 22 March 2010, revised 21 June 2010
Uspekhi Fizicheskikh Nauk **180** (10) 1009 – 1034 (2010)
DOI: 10.3367/UFNr.0180.201010a.1009
Translated by Yu V Morozov; edited by A M Semikhatov

1. Introduction

The physics of magnetism distinguishes between weak and strong magnetic substances depending on the degree of their magnetic susceptibility. Strongly magnetic matter does not occur in nature in the liquid state, but synthetic magnetic fluids (MFs) exhibiting strong magnetic properties have been studied and used for more than 40 years. Such magnetic fluids, or ferrofluids, are highly dispersed systems of ferromagnetic or ferrimagnetic particles in a liquid medium (organic or inorganic fluids, water) [1, 2]. Each particle is coated with one or several layers of surface-active agents (surfactants) that separate the particles and prevent their adhesion (Fig. 1). The resultant two-phase liquid medium is stable but very susceptible to external magnetic fields and has properties resembling those of a homogeneous fluid. The main characteristic feature of an MF is the size of dispersed particles, varying from 3 to 20 nm or more depending on the magnetic material used. It is this characteristic, along with the proper choice of the surfactant, that accounts for the high MF stability [3, 4]. Magnetic fluids do not undergo phase separation in an external magnetic field and completely recover their initial properties after the field is removed. This property distinguishes MFs from magnetic suspensions (magnetorheologic fluids) composed of 1–10 μm particles. Magnetic suspensions almost solidify under the effect of an applied magnetic field (a property extensively used for a variety of purposes) and their aggregated particles need to be redispersed into the liquid medium to make them suitable for further utilization. From the physical standpoint, this difference is attributable to the fact that the energy of attraction between colloidal particles in an MF (magnetic interaction plus van der Waals interaction) is close to the particle thermal energy (Brownian repulsion). Another important characteristic of MFs is the single-domain state of spontaneous magnetization particles determined by their size, which accounts for the quasi-paramagnetic behavior of MFs.

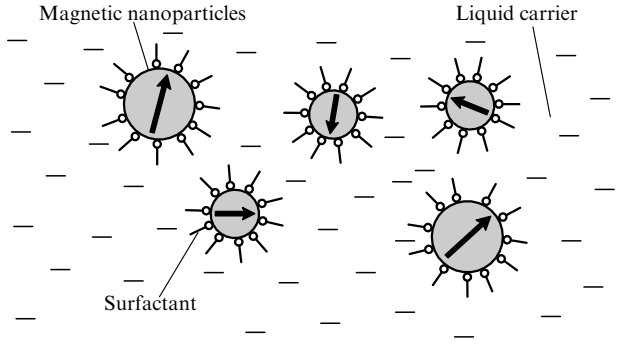

Figure 1. Principal diagram of the magnetic fluid structure. The characteristic size (2–20 nm) of surfactant-coated magnetic particles corresponds to their single-domain magnetization state indicated by arrows.

Investigations of liquid systems of particles with magnetic dipole–dipole interactions gave rise to a new scientific discipline, magnetic hydrodynamics [1–3, 5–7].

The volume fraction of magnetic particles in a highly stable MF amounts to 25%. Magnetic fluids exhibit a variety of unusual properties due to a combination of magnetism and fluidity. When the particle–particle attraction-to-repulsion ratio in the system is slightly higher than unity, the application of an external magnetic field induces specific aggregation of nanoparticles into linear chains arrayed parallel to the field. Such aggregation dramatically alters the MF properties, making them anisotropic with respect to the field direction; this, in turn, changes practically all the physical characteristics of MFs including density, viscosity, surface tension, conductivity, and inductivity; this implies the possibility of controlling MF properties by varying the external magnetic field. The above properties account for the wide application of MFs in various technical devices [3, 8]. An MF can be used as a medium for the storage and subsequent modification (functionalization) of magnetic nanoparticles for such rapidly developing fields as nanoelectronics [9–11] and biomedicine [12–18].

Both MF research and practical application pose a serious problem concerning the preparation and stability of compositions with the desired controllable properties. This problem, common for nanosystems, is in fact related to the dynamic stability of self-organized systems. Of primary importance for its resolution are structural studies aimed at determining the parameters of the atomic and magnetic structure of MF particles, their interaction potential, and the effect of external magnetic fields on these characteristics.

Neutronography [19–27] has greatly contributed to the development of the MF structural analysis. The small-angle neutron scattering (SANS) method is widely used in the MF research, because it allows an in-depth study of the MF microstructure and its comparison with the macroscopic properties of MFs. The main factors predetermining successful application of neutronography are the possibility of applying the contrast technique using the hydrogen ↔ deuterium isotopic substitution and the phenomenon of magnetic interaction between neutrons and magnetic atoms. By virtue of the high neutron penetrability, this method does not require special preparation of samples under study; typically, unmodified and bulk (e.g., industrial) systems prepared by a standard procedure are investigated.

Progress in the use of SANS for the MF research primarily occurs because these systems have a well-defined and relatively simple structure (see Fig. 1). The homogeneous basis of such systems (a liquid carrier) distinguishes them from solid magnetic nanocomposite materials, such as magnetic polymer composites and ferrogels [28], whose matrices are in themselves sources of strong coherent scattering due to their inhomogeneous structure. A liquid carrier medium provides wide opportunities for realizing contrast variation in the MFs of interest using mixtures of deuterated (D) and nondeuterated (ND) fluids that retain their properties. The hierarchical structure of information that can be obtained by the SANS technique is schematically shown in Fig. 2. Implementation of this scheme greatly promoted the understanding of the physical mechanisms of MF stabilization and the development of specific recommendations for manufacturers [4, 29–34].

At the same time, interpretation of neutron scattering on MFs poses a number of methodological problems. Magnetic nanoparticles dispersed into a liquid carrier usually show strong polydispersity, which complicates the analysis of experimental data. Moreover, polydispersity is difficult to

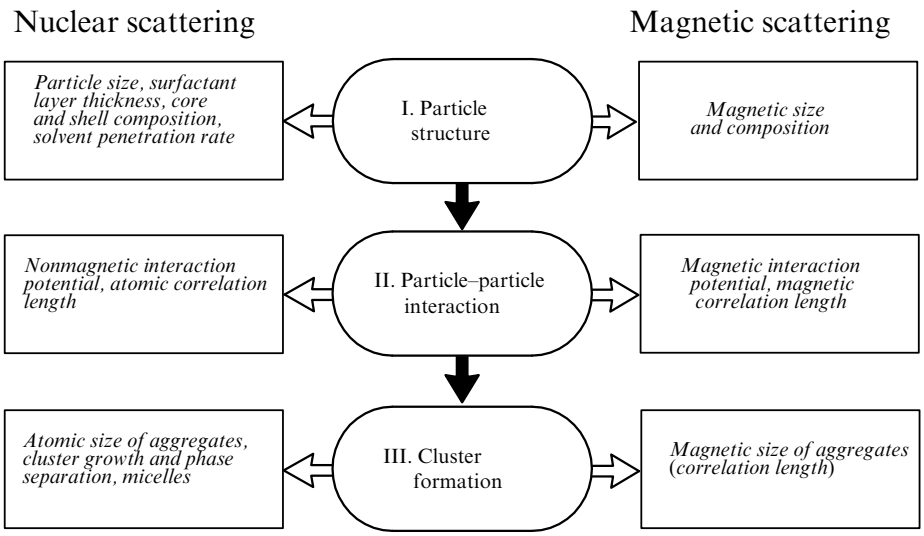

Figure 2. Hierarchical structure of the information on the MF microstructure obtainable by neutron scattering.

take into account because MFs exhibit a strong dipole–dipole interaction between the particles that depends on the mutual orientation of their magnetic moments and leads to deviations from the purely paramagnetic behavior. Active MF research using SANS initiated the development of the contrast variation technique for the study of polydisperse and magnetic particles and the polarized neutron scattering method. Both methods provide differential information about nuclear and magnetic scattering. All these issues are common for nanoparticle solutions. Hence, there is the long-felt need to summarize the results of SANS application to the MF research.

This review of SANS-based investigations reported in the last 20 years is designed to elucidate the potential of this method for the MF research and to discuss prospects for its further development. Special emphasis is laid on the comparison of SANS and other complementary methods used in structural studies, e.g., the X-ray (synchrotron) scattering technique.

The review is organized as follows. Section 2 contains a description of the main types of study systems and a brief introduction to the SANS method, with special reference to its application to magnetic nanoparticle research. An extension of the contrast variation technique to the structure research of polydisperse MFs is proposed in Section 3. The so-called direct analysis of SANS scattering curves in the framework of different models is discussed in Section 4. The cases of noninteracting and interacting (up to cluster formation) particles in nonmagnetized MFs are considered in Section 4. Section 5 is focused on the use of nonpolarized and polarized neutrons in SANS for the structural analysis of magnetized MFs.

2. Subject and method of research

2.1 Main types of magnetic fluids

A large variety of spontaneously magnetized substances, including iron oxides (magnetite, maghemite), cobalt, and nickel compounds, are used as dispersable magnetic materials in MFs. Synthesis of MFs containing nanoparticles of pure metals resulting in a substantial enhancement of magnetic interactions imposes increased requirements for the stabilization of such systems. The precipitation reaction is the most popular tool for preparing a disperse system of magnetic nanoparticles (see, e.g., [4]). Under certain conditions, magnetite particles from 2 to 20 nm in size are formed in an aqueous mixture of di- and tri-valent iron salts; they are further transferred into different liquid media by special chemical procedures. The description of other methods for the production of magnetic nanoparticles for MFs (thermal decomposition, laser pyrolysis) can be found in specialized reviews (see, e.g., Ref. [4]).

There are several ways to stabilize an MF. The structure of the corresponding particles is shown in Fig. 3. Stabilization in nonpolar organic solvents (benzene, hexane, toluene, decalin) is achieved by hemosorption of a single surfactant layer at the surface of the magnetic particles (Fig. 3a) [1, 31, 34, 35]. A classical surfactant for the purpose is oleic acid ($C_{18}H_{34}O_2$), an unsaturated monocarboxylic acid whose molecule roughly 1.8 nm in length is bent at the carbon–carbon double bond in the middle. Such a coating ensures a sufficient nonelectrostatic (steric) repulsion between particles. Importantly, they can be redispersed by flocculation

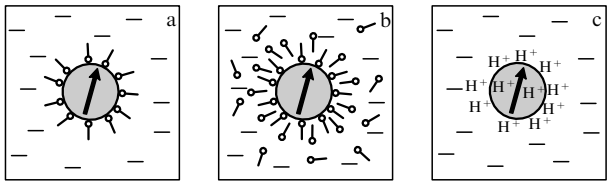

Figure 3. Main types of MF stabilization: (a) single steric, (b) double steric, (c) ionic (electrostatic).

(acetone) into any similar medium without a substantial loss of the concentration and stability.

Interaction between the surfactant lyophilic head and the fluid in polar liquid bases, including water, competes with absorption of the surfactant head at the surface of magnetic particles. Surfactant desorption is prevented by double steric stabilization [29, 30, 32, 36–38] for which particles with a single surfactant layer are coated by physical absorption of the second one (Fig. 3b). An excess of the second surfactant in the solution is needed for the purpose. Such stabilization cannot be completely steric because of the polarity of both solution components, the solvent and the surfactant. There is always a certain induced charge at the shell–solvent interface that makes an additional contribution to stabilization through the formation of a double electric layer around particles [39, 40]. A purely electrostatic stabilization can be realized in an aqueous base (Fig. 3c) due to the presence of H^+ and OH^- ions or ion-containing groups [e.g., citrate ions $C_3H_5O(COO)_3^{3-}$] at the surface of magnetic particles [41, 42]. This class of MFs is highly sensitive to the pH and ionic strength of the liquid base [43, 44].

Some authors have attempted to use different polymers to form a stabilizing coating around magnetic particles (largely for biomedical applications) [45, 46]. The interest in this type of stabilization is due to two factors. First, polymer-coated particles are easier to functionalize (i.e., to attach chemical groups necessary for the desired applications). Second, particles administered into a living organism must be biocompatible (i.e., induce neither immune reactions nor toxic responses); this goal is most efficiently achieved by using relevant polymer molecules.

Understanding the physical mechanisms underlying the MF stabilization is an important condition for the development of synthesis of new MF classes with predetermined and adjustable properties. The colloidal nature of MF solutions suggests cluster formation both in the presence and in the absence of an external magnetic field. The aim of MF stabilization is to make this process practicable and controllable. The use of chained aggregates of MF particles formed in an external magnetic field has already been mentioned in the Introduction. The formation of compact and branched (fractal) clusters may seem a negative factor reducing the MF stability. But such clusters may prove to be of value in various applications, e.g., sorting out magnetic materials [47]. Their main characteristic is demagnetization after removal of the magnetic field. It allows easily (compared with the same procedure in suspensions) separating the MF from other magnetic materials and reutilizing it if appropriate.

2.2 Principles of small-angle scattering

The evolution of small-angle scattering techniques, including SANS, can be traced from [20, 48–51]. In the present section,

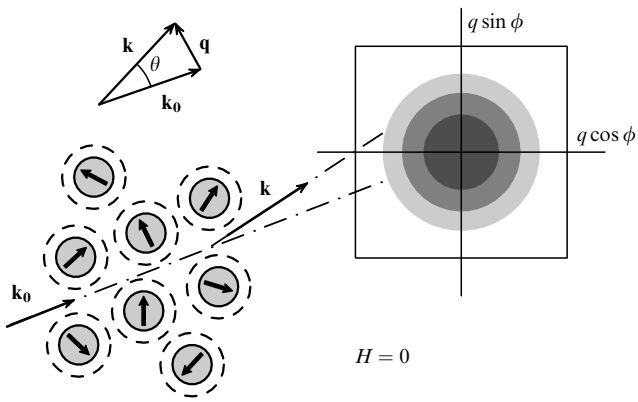

Figure 4. Principal diagram of a SANS experiment with MFs in the absence of an external magnetic field in the sample. Magnetic moments of the particles have arbitrary directions.

the basic classical principles are considered; further development of the method for the purpose of the MF structure research is considered in Sections 3–5.

2.2.1 Main notions and formulas. A SANS experiment analyzes the broadening of a beam of thermal neutrons (with the wavelength 0.1–1 nm) after it passes through a sample as a result of elastic scattering on 1–100 nm inhomogeneities (Fig. 4). Unlike X-ray (synchrotron) radiation scattered on electron shells, neutrons interact with atomic nuclei. The character of this interaction is described by a tabulated parameter, the scattering length b_{N}. Coherent and incoherent neutron scattering lengths are distinguished. Coherent scattering corresponds to the scattering affected by interference and may therefore be regarded as informative for the purpose of structural analysis. Incoherent scattering is a result of several stochastic factors (the difference between spin orientations of neutrons and nuclei, isotopic distribution of the nuclei) responsible for the somewhat disturbed scattering interference. The isotropic incoherent constituent is the source of a sort of background in neutron experiments. Hydrogen nuclei are the main contributors to this component. The incoherent scattering cross section of other elements is more than 10 times smaller; therefore, the substitution of deuterium for hydrogen significantly reduces the incoherent background in experiments. Incoherent scattering is associated not only with true absorption of neutrons involved in nuclear reactions (generally rather weak for thermal neutrons) but also with an additional weakening of the neutron beam passing through the study system. Its weak dependence on the neutron wavelength allows using cold neutrons (with a wavelength more than 1 nm) in SANS experiments and thereby widening the range of correlations being studied to more than 100 nm. Such a possibility distinguishes neutron scattering techniques from the X-ray (synchrotron) radiation method, in which intense absorption of all elements occurs at large wavelengths. In what follows, the coherent length is meant by scattering length.

Another fundamental difference between neutron and X-ray (synchrotron) radiation is that neutrons have an intrinsic magnetic moment (the neutron spin is 1/2). An additional interaction of neutrons with the electron shell of an atom acquires significance; in the first approximation, it is described by the magnetic scattering length b_{M}. Indices N and M are used below to denote nuclear and magnetic scattering.

The aim of a SANS experiment is to determine, from the differential cross section, the distribution $\rho(\mathbf{r})$ of nuclear and magnetic scattering length densities (SLDs) inside inhomogeneities, and to describe possible correlations between inhomogeneities for different parameters (location, orientation, magnetization, and so on). The differential thermal neutron (hereinafter, neutron) scattering cross section $\mathrm{d}\sigma/\mathrm{d}\Omega$ is a function of the scattering vector $\mathbf{q} = \mathbf{k} - \mathbf{k}_0$, which is the difference between the wave vectors of the incident ($\mathbf{k}_0$) and scattered ($\mathbf{k}$) beams. The scattering being elastic on the whole, the relation

$$q = \frac{4\pi}{\lambda} \sin \frac{\theta}{2} \tag{1}$$

for the scattering vector modulus holds, where λ is the neutron wavelength and θ is the scattering angle. In the case of neutron magnetic scattering, its length b_{M} depends on the angle α between the atom magnetic moment and the vector $\mathbf{q}$ as

$$b_{\mathrm{M}} = b_{\mathrm{M}}^{0} \sin \alpha \,, \tag{2}$$

where b_{M}^{0} is calculated from the corresponding term of the magnetic atom.

The differential scattering cross section and the SLD distribution are related through the scattering amplitude, i.e., the Fourier transformation of the SLD distribution:

$$F_{\mathrm{N,M}}(\mathbf{q}) = \int_V \rho_{\mathrm{N,M}}(\mathbf{r}) \exp\left(\mathrm{i}\mathbf{q}\mathbf{r}\right) \mathrm{d}\mathbf{r} \,. \tag{3}$$

Here, the integral is taken over the entire (coherent) volume of the system of interest (for neutrons, of the order of 1 $\mu\mathrm{m}^3$). For the differential cross section, we have

$$\frac{\mathrm{d}\sigma}{\mathrm{d}\Omega_{\mathrm{N,M}}}(\mathbf{q}) = \left|F_{\mathrm{N,M}}(\mathbf{q})\right|^2 = \int_V \int_V \rho_{\mathrm{N,M}}(\mathbf{r}_1)\, \rho_{\mathrm{N,M}}(\mathbf{r}_2) \exp\left(\mathrm{i}\mathbf{q}(\mathbf{r}_1 - \mathbf{r}_2)\right) \mathrm{d}\mathbf{r}_1\, \mathrm{d}\mathbf{r}_2 \,. \tag{4}$$

When the study system is isotropic (with respect to both nuclear and magnetic scattering components, as shown in Fig. 4), the experiment measures the one-dimensional function of the scattering vector modulus $\langle \mathrm{d}\sigma/\mathrm{d}\Omega(\mathbf{q})\rangle_{\Omega} = \mathrm{d}\sigma/\mathrm{d}\Omega(q)$, and hence (4) is simplified to

$$\frac{\mathrm{d}\sigma}{\mathrm{d}\Omega_{\mathrm{N}}}(q) = \int_V \int_V \rho_{\mathrm{N}}(\mathbf{r}_1)\, \rho_{\mathrm{N}}(\mathbf{r}_2)\, \frac{\sin\left(q|\mathbf{r}_1 - \mathbf{r}_2|\right)}{q|\mathbf{r}_1 - \mathbf{r}_2|}\, \mathrm{d}\mathbf{r}_1\, \mathrm{d}\mathbf{r}_2 \,, \tag{5a}$$

$$\frac{\mathrm{d}\sigma}{\mathrm{d}\Omega_{\mathrm{M}}}(q) = \frac{2}{3} \int_V \int_V \rho_{\mathrm{M}}(\mathbf{r}_1)\, \rho_{\mathrm{M}}(\mathbf{r}_2)\, \frac{\sin\left(q|\mathbf{r}_1 - \mathbf{r}_2|\right)}{q|\mathbf{r}_1 - \mathbf{r}_2|}\, \mathrm{d}\mathbf{r}_1\, \mathrm{d}\mathbf{r}_2 \,. \tag{5b}$$

In (5b), the magnetic component factor 2/3 is singled out as a result of averaging b_{M}^2 [see relation (2)] over all orientations of the magnetic moments relative to $\mathbf{q}$. The double integral in (5a) or (5b) is known as the Debye formula [49], which allows parameterization of scattering and fitting to experimental scattering curves $\mathrm{d}\sigma/\mathrm{d}\Omega(q)$.

In what follows, we omit the indices N and M unless this leads to misunderstanding, and write formulas for nuclear scattering alone. To pass to magnetic scattering in an isotropic case, the scattering cross section should be multiplied by 2/3.

The practical aspects of the realization of the principal diagram of the SANS experiment presented in Fig. 2 are

considered in Refs [49, 50]. Selection of small scattering angles θ (0.05 rad or less) requires rather strong collimation using large path lengths (1–30 m) between the beam-forming collimators and between the sample and the detector. An important component of SANS units is a planar position-sensitive detector having a large area (from 50×50 cm^2 to 120×120 cm^2) that encompasses a large solid angle in one dimension. The resolution of thermal neutron detectors used in practical work (from 2×2 mm^2 to 10×10 mm^2), the collimation resolution (0.5–5 cm), and the wavelength resolution (10–20%) are chosen by reference to the optimal q resolution (5–30%) determined by neutron fluxes from their modern sources [27]. At present, the optimal regime of SANS experiments in the leading world neutron centers [22, 27] ensures fluxes of $10^6 - 10^7$ cm^{-2} s^{-1} on a sample, which determine characteristic times of experiments in a range from tens of minutes to several hours (depending on the scattering cross section being measured). Such fluxes allow effectively using axially symmetric (pin-hole) geometry for collimation. In this case, the corresponding resolution (instrument) function is rather symmetric and close to the Gaussian distribution, which is relatively easy to take into account when treating the scattering curves [51, 52]. As follows from (1), scanning over q is possible by varying both the scattering angle θ (the steady-state regime on continuous neutron sources) and the neutron wavelength λ (the time-of-flight regime on pulsed neutron sources). These two methods are not essentially different in terms of obtaining and subsequently treating the scattering curves $\mathrm{d}\sigma/\mathrm{d}\Omega(q)$.

2.2.2 Scattering on isolated nanoparticles. When the inhomogeneities exist as well-defined and identical spatial regions [e.g., nanoparticles in a certain homogeneous matrix (solvent), noninteracting and chaotically distributed over shape anisotropy orientations], expression (5) can be rewritten taking the scattering on the solvent into account:

$$\frac{\mathrm{d}\Sigma}{\mathrm{d}\Omega}(q) = I(q) = n \int_{V_0} \int_{V_0} \big(\rho(\mathbf{r}_1) - \rho_\mathrm{s}\big)\big(\rho(\mathbf{r}_2) - \rho_\mathrm{s}\big) \times \frac{\sin\big(q|\mathbf{r}_1 - \mathbf{r}_2|\big)}{q|\mathbf{r}_1 - \mathbf{r}_2|}\, \mathrm{d}\mathbf{r}_1\, \mathrm{d}\mathbf{r}_2 = nP(q)\,, \tag{6}$$

where $\mathrm{d}\Sigma/\mathrm{d}\Omega(q)$ is the differential scattering cross section per unit volume of the sample (by convention, it is referred to as the scattering intensity $I(q)$ in what follows); ρ_s is the corresponding (nuclear or magnetic) SLD of the solvent; V_0 is the nanoparticle volume; and n is the particle number density in the medium. The double integral in (6), denoted as $P(q)$, has the meaning of the particle form factor (differential scattering cross section on a single particle). An essential feature of (6) is the transition to integration over a single particle volume with the simultaneous substitution of the SLD in the sample volume in (5) by differences $\rho(\mathbf{r}) - \rho_\mathrm{s}$ that determine the scattering capacity of the particles and their individual components against the solvent (contrast).

An important characteristic of expression (6) for the form factor is that the scattering that can be reliably (with a large signal-to-noise ratio) recorded concentrates in the small-q region corresponding to the condition

$$q \sim \frac{2\pi}{D}\,, \tag{7}$$

where D is the characteristic size of the particle.

In the case of spherically isotropic particles, $\rho(\mathbf{r}) = \rho(r)$; in other words, the form factor is directly related to the scattering amplitude as

$$P(q) = F^2(q)\,, \tag{8}$$

$$F(q) = 4\pi \int_0^{R_\mathrm{max}} \big(\rho(r) - \rho_\mathrm{s}\big)\, \frac{\sin(qr)}{qr}\, r^2\, \mathrm{d}r\,, \tag{9}$$

where R_max is the particle maximum radius.

Scattering curve (6) can be analyzed using scattering invariants (integral parameters). For example, Guinier's law holds at sufficiently small q regardless of the SLD distribution:

$$I(q) \underset{q\to 0}{=} I(0) \exp\left(-\frac{1}{3} R_\mathrm{g}^2 q^2\right), \tag{10}$$

where $I(0)$ is the forward scattering intensity and R_g is the gyration radius of the SLD distribution inside the particle,

$$R_\mathrm{g}^2 = \frac{\int_{V_0} \big(\rho(\mathbf{r}) - \rho_\mathrm{s}\big) r^2\, \mathrm{d}\mathbf{r}}{\int_{V_0} \big(\rho(\mathbf{r}) - \rho_\mathrm{s}\big)\, \mathrm{d}\mathbf{r}}\,. \tag{11}$$

The Guinier law is obeyed at $qR_\mathrm{g} < 1$. For completely homogeneous particles with a density ρ,

$$I(0) = nV_0^2(\rho - \rho_\mathrm{s})^2 = \varphi V_0(\rho - \rho_\mathrm{s})^2\,, \tag{12}$$

where φ is the volume fraction of the particles in the solution and the difference $\rho - \rho_\mathrm{s}$ is the particle contrast. Evidently, the absolute SLD value is unessential because the key factor is the difference between the particle and the medium SLDs, while it is impossible to say which density is greater because of the quadratic contrast dependence in SANS experiments. The situation in which a particle placed in a nonzero SLD medium has zero SLD (i.e., fails to scatter neutrons) is equivalent to the situation with similar particles having a nonzero SLD in the vacuum. The contrast dependence of (12) is actually a reflection of Babinet's principle, well-known in the diffraction theory [49]. The gyration radius of a homogeneous particle is directly related to its shape. Parameters of a putative shape are estimated from an experimental R_g value [20, 49].

For homogeneous particles, the Porod integral (invariant) is informative:

$$Q = \int_0^\infty I(q) q^2\, \mathrm{d}q = 2\pi^2 n V_0 (\rho - \rho_\mathrm{s})^2\,. \tag{13}$$

The particle volume is found by simultaneously solving (12) and (13):

$$V_0 = 2\pi^2 \frac{I(0)}{Q}\,. \tag{14}$$

In the general case, relation (14) is called the Porod volume. The scattering invariants (Guinier parameters and Porod volume) for nonhomogeneous particles are discussed at greater length in Section 5.

If particles have several characteristic dimensions, then the corresponding inflection points can be distinguished on the scattering curve based on the Guinier approximation. For strongly anisotropic 'rod-like' or 'disk-like' particles, there are two characteristic dimensions (length and diameter for

'rods,' diameter and thickness for 'disks') for which such points exist. The power-law relation between them,

$$I(q) \sim \frac{A}{q^{\alpha}}\,, \tag{15}$$

is fulfilled with good accuracy; here, A is a certain constant, and the exponent α takes the respective values 1 and 2 for prolate ('rod-like') and oblate ('disk-like') particles. The power law can also manifest itself in other cases, as discussed in this section below and in Section 2.2.3. The possible values of α are presented in Table 1.

Table 1. Interpretation of the exponent of the power-law dependence of scattering (15).

α	Structure
$\alpha = 1$	Prolate particle
$\alpha = 2$	Oblate (flattened) particle
$1 < \alpha < 3$	Mass fractal, dimension $D = \alpha$
$3 < \alpha < 4$	Fractal surface, dimension $D_s = 6 - \alpha$
$\alpha = 4$	Smooth surface, $D_s = 4$ (Porod law)
$4 < \alpha < 6$	Diffuse surface, $\alpha = 4 + 2\beta$

In the limit $q \to \infty$ corresponding to scattering on a particle surface, the intensity also obeys a power law,

$$I(q) \underset{q\to\infty}{\sim} \frac{B}{q^{\alpha}}\,, \tag{16}$$

where B is a constant and the exponent α takes values from 3 to 6. The range $3 < \alpha < 4$ corresponds to the so-called fractal surface characterized by a fractal dimension D_s [52–56]. In the general case, the dimension D is introduced through the number of structural units N enclosed in a sphere of radius r [57, 58]:

$$N(r) \sim \left(\frac{r}{R_0}\right)^{D}\,, \tag{17}$$

where R_0 is the structural unit radius. It follows from (17) that for a particle of an arbitrary shape with the fractal surface, the SLD averaged over all orientations of the particle as a function of radius has the following form at the surface:

$$\rho(r) \sim r^{D_s - 3}\,. \tag{18}$$

The corresponding Fourier transformation gives a relation between the surface fractal dimension and the exponent α:

$$D_s = 6 - \alpha\,. \tag{19}$$

Relation (19) is satisfied in the range $\pi/R_0 < q < 2\pi/d_{\text{in}}$, where d_{in} is the characteristic interface thickness (characteristic size of surface inhomogeneities).

We note for completeness that another range, $4 < \alpha < 6$, corresponds to the so-called diffuse surface [55]. The respective function of SLD at the interface has a singularity of a different form:

$$\rho(r) = \rho\left(\frac{R_{\max} - r}{a}\right)^{\beta}, \qquad R_{\max} - a < r < R_{\max}\,, \tag{20}$$

where ρ refers to the homogeneous 'core' of the particle, a defines a certain effective thickness of the interface, and the exponent β takes values in the range $0 \leqslant \beta < 1$. At the point $r = R_{\max}$, the SLD of form (20) has an infinite derivative. The corresponding relation to the exponent α in (16) is expressed as

$$\alpha = 4 + 2\beta\,. \tag{21}$$

We note that for particles of a symmetric near-spherical shape, expression (16) should be regarded as describing the asymptotic behavior of the scattering curve. In the case of more branched (asymmetric) or polydisperse particles, the scattering curves display a well-apparent power-law dependence. The case $\alpha = 4$, corresponding to a smooth surface, is known as Porod's law.

Representation of expression (6) in direct space is also used in the analysis of scattering:

$$I_{\text{N,M}}(q) = 4\pi \int_0^{\infty} p_{\text{N,M}}(r)\, \frac{\sin(qr)}{qr}\, \mathrm{d}r\,, \tag{22}$$

where the transition to spherical coordinates is additionally realized. The function $p(r)$ can be found from the experimental scattering intensity by indirect Fourier transformation [49, 51], a special procedure for smoothing small-angle scattering data. Similarly to $I(q)$, the function $p(r)$ has specific features giving an idea of the SLD within a particle. For completely homogeneous and monodisperse particles, $p(r)$ has the meaning of a pair distance distribution density inside a particle.

We note that the presence of polydisperse particles with a certain distribution over the radius, $D_n(R)$, substantially complicates the interpretation of scattering. For example, an additional integration must be introduced in (6):

$$I(q) = n \int_0^{R_{\max}} P(q, R)\, D_n(R)\, \mathrm{d}R\,, \tag{23}$$

where the dependence of the form factor of an individual particle on its size $D_n(R)$ is explicitly indicated and n has the meaning of the mean particle number density, $n = \varphi/\langle V\rangle$. Given the known form factor $P(q, R)$, it is possible to find $D_n(R)$. The aforementioned indirect Fourier transformation [49, 51] is extensively used along with direct simulation (23).

As follows from (4), the scattering cross section in the general case is anisotropic, i.e., independent of the direction of the vector $\mathbf{q}$ with respect to the particle anisotropy axis. For the analysis of scattering in accordance with (4) in the general case of noninteracting particles, they must be oriented in one direction in terms of both shape anisotropy and magnetization (for magnetic particles). The analysis of anisotropic nuclear scattering is a challenging task (actually, a separate case of SANS applications). The present review is focused on particles similar to spherically isotropic ones. The anisotropy of the magnetic form factor is in a sense easier to interpret because it is described by a well-defined and simple formula. For ordering the magnetic moments of particles unidirectionally, experiments are carried out in the external saturation magnetic field. In this case, the nuclear component of scattering may remain isotropic, making it possible to discriminate between the two components. The efficiency of such differentiation is increased by using polarized neutrons, as is discussed and demonstrated in Section 5.

2.2.3 Effect of the interaction. As the volume fraction of particles in a system becomes higher than $\varphi \sim 5\%$, the effect of interparticle interaction becomes essential for the scatter-

ing. This effect may also be manifested at lower concentrations in the case of additional interactions (the strong van der Waals dispersion interaction, the surface electrostatic Coulomb interaction, the magnetic attraction for magnetic particles). In such cases, the positions and orientations of particles can no longer be regarded as independent because of a correlation between the particles. The correlation length is comparable with the particle size; therefore, the corresponding scattering may occur in the region of small q values. In the case of an isotropic interaction between monodisperse particles, the corresponding effect factors [i.e., the so-called structure factor $S(q)$ appears together with the form factor $P(q)$ in expression (6)]:

$$I(q) = nP(q)\,S(q)\,. \tag{24}$$

As the concentration decreases, $S(q)$ tends to unity. The structure factor is a Fourier transform of the radial distribution function $g(r)$:

$$S(q) = 1 + 4\pi n \int_0^\infty \big(g(r) - 1\big)\,\frac{\sin(qr)}{qr}\,r^2\,\mathrm{d}r\,. \tag{25}$$

The function $g(r)$ is defined as the time-averaged radial distribution function of particles around a distinguished particle depending on its radius measured from the center. In fact, $g(r)$ reflects the density modulation resulting from the particle–particle interaction; in other words, it characterizes the appearance of the short-range order inherent in liquids at the atomic level. According to the theory of liquids, the function $S(q)$ can be computed from the Ornstein–Zernike equation, which includes the particle–particle interaction potential. In the general case, solving this equation is an extremely difficult task. There are only few cases where it is possible to obtain an explicit dependence of $S(q)$ on the interaction potential parameters by using a number of simplifying assumptions. The situation is further complicated for polydisperse and anisotropic particles, as we show in Sections 4 and 5.

A certain correlation between particles also occurs in the case of their aggregation (clusterization, polymerization). For example, expression (17) involving the fractal organization of a cluster (mass fractal) holds equally well for both the interface and the whole cluster. In this case, R_0 is understood as the characteristic radius of nanoparticles making up the cluster. A power law of form (16) is identified on the scattering curve, as in the case of a surface, but the exponent α corresponds to the mass (bulk) fractal dimension of the cluster [55, 56, 59, 60]:

$$D = \alpha\,. \tag{26}$$

The corresponding observational interval (16) is $\pi/R_0 > q > \pi/R_{\mathrm{cl}}$, where R_0 is the characteristic particle radius and R_{cl} is the cluster size. This case is also included in Table 1.

2.3 Peculiarities of small-angle neutron scattering on magnetic nanoparticles

As mentioned above, the magnetic component (a result of interactions between the magnetic moments of neutrons and particles) is added to the nuclear component. For the purpose of the primary estimation of the structural parameters of colloid particles (magnetic nanoparticles plus a surfactant shell) in a low-concentration MF (with the volume fraction of magnetic material $\varphi_{\mathrm{m}} < 3\%$), it is possible to neglect interference effects due to interparticle interaction and regard the magnetic fluid as a system of noninteracting particles. In the absence of an external magnetic field, magnetic moments of nanoparticles in the MF have arbitrary directions, which makes the two scattering components isotropic with respect to the direction of the vector $\mathbf{q}$, as shown in the principal diagram in Fig. 4. Because disperse particles in the MF have a quasi-spherical shape, it is possible to write the differential scattering cross section on a single particle, in accordance with (5) and (7), as

$$I(q) \approx F_{\mathrm{N}}^2(q) + \frac{2}{3}\,F_{\mathrm{M}}^2(q)\,, \tag{27}$$

where F_{N} and F_{M} are nuclear and magnetic scattering amplitudes.

Figure 5 is a model representation of the 'nuclear' (in fact, atomic) and magnetic form factors for an individual particle in an MF. For the 'nuclear' form factor, the 'sphere-shell' model gives

$$F_{\mathrm{N}}^2(q) = \big[(\rho_0 - \rho_1)\,V_0\Phi(qR_0) + (\rho_1 - \rho_{\mathrm{s}})\,V_1\Phi(qR_1)\big]^2\,, \tag{28a}$$

$$\Phi(x) = \frac{3\big(\sin x - x\cos x\big)}{x^3}\,. \tag{28b}$$

Here, ρ_0, ρ_1, and ρ_{s} are the respective nuclear scattering length densities of the central 'sphere' (magnetic nanoparticle), the surfactant shell, and the solvent (liquid carrier); in Fig. 6, their values are calculated from the density characteristics of typical materials; and V_0 and V_1 are the volumes limited by the radii R_0 and R_1. The difference $h = R_1 - R_0$ defines the effective surfactant shell thickness.

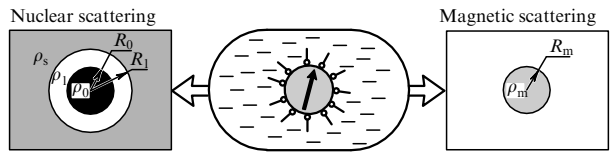

Figure 5. Model representation for the 'nuclear' and magnetic particle structures in an MF from the standpoint of neutron scattering.

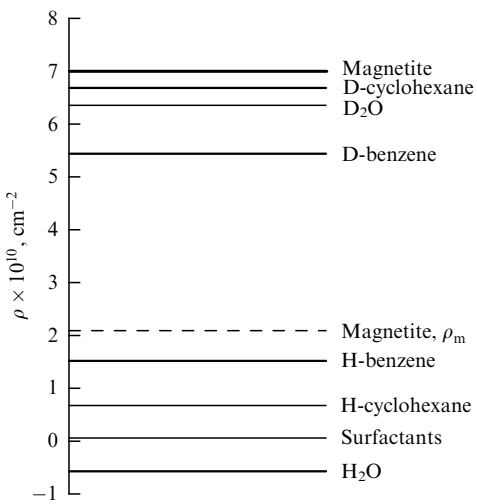

Figure 6. Schematic of nuclear SLDs of different MF components. Dashed line shows the magnetic SLD of magnetite (upper bound).

The surfactant shell and the liquid medium being nonmagnetic, the magnetic form factor of the particles must be described by a simpler formula corresponding to the spherical model:

$$F_{\mathrm{M}}^2(q) = \rho_{\mathrm{m}}^2 V_{\mathrm{m}}^2 \Phi^2(qR_{\mathrm{m}})\,. \tag{29}$$

Here, ρ_{m} is the magnetic SLD of a nanoparticle distributed within the volume V_{m} with the respective radius R_{m}. The density ρ_{m} can be calculated from the substance crystalline structure. We note that the magnetic scattering length used in this case depends on the spin–orbital interaction. In certain cases (e.g., the Fe^{3+} state in magnetite), there are different estimates of this interaction, which leads to an ambiguity in ρ_{m} and makes this parameter uncertain. Also, it is assumed that R_{m} differs from R_0 due to formation of a nonmagnetic layer at the nanoparticle surface due to deviations of atomic spin moments from the domain magnetization direction at the interface. Different experiments, including those on magnetization analysis [61–64], the Mössbauer effect [65, 66], and the structural diffraction of polarized neutrons [67], give estimates of the thickness of this layer $\delta = 0.1-0.8$ nm. The spin deviations under discussion were qualitatively confirmed by calculations in [68]. However, direct experimental evidence of a nonmagnetic surface layer in magnetic nanoparticles remains to be obtained. A decrease in the magnetic moment in the entire nanoparticle volume may be an alternative explanation of the low specific magnetization [69–71].

For most MFs, there is a certain relation between their components and the SLD. Figure 6 compares the SLDs of magnetic fluids and liquid H- and D-bases; in addition, it shows the characteristic magnetic SLD of magnetite. H-bases and surfactant shells have similar SLDs, while D-bases are closer to magnetic cores of complex particles in terms of this parameter. In Section 3, we consider the possibilities of a common approach to the analysis of scattering curves for MFs upon SLD variation in the liquid base (contrast variation). The results obtained are further compared with the data of direct analysis of the scattering curves for nonmagnetized (Section 4) and magnetized (Section 5) MFs.

3. Contrast variation in the scattering by polydisperse superparamagnetic systems

3.1 The classical approach for monodisperse nonmagnetic systems

Contrast variation is the classical method in SANS experiments. It is based on the analysis of changes in the scattering curve with a variable contrast $\Delta\rho$ (the difference between the mean scattering length of the particles $\bar{\rho}$ and the scattering length of the homogeneous medium ρ_{s} containing these particles):

$$\Delta\rho = \bar{\rho} - \rho_{\mathrm{s}}\,. \tag{30}$$

In the general case, contrast variations in a system of noninteracting particles are interpreted in terms of the basic function approach proposed by Stuhrmann in the late 1960s [72, 73]. This approach is applicable to the systems of monodisperse and identical nonmagnetic particles that are assumed to be nonmagnetic. Then the scattering intensity can be represented as a series in powers of the contrast:

$$I(q) = I_{\mathrm{s}}(q) + \Delta\rho\, I_{\mathrm{cs}}(q) + (\Delta\rho)^2 I_{\mathrm{c}}(q)\,, \tag{31}$$

where $I_{\mathrm{c}}(q)$, $I_{\mathrm{cs}}(q)$, and $I_{\mathrm{s}}(q)$ are the so-called basic functions. The function $I_{\mathrm{c}}(q)$ corresponds to the shape scattering of a single particle, $I_{\mathrm{s}}(q)$ corresponds to the scattering on density fluctuations (inhomogeneities) inside the particle, and $I_{\mathrm{cs}}(q)$ defines interference between the two contributions. The basic functions can be found in experiment from $I(q)$ measurements at different contrast values. In neutron scattering experiments, the contrast in a system is typically altered by varying the density ρ_{s} by means of hydrogen–deuterium isotopic substitution. A review of classical studies using this approach to investigate monodisperse biological macromolecules and complexes can be found in Ref. [74].

The behavior of basic functions in the vicinity of zero determines the contrast dependences of the integral parameters of the scattering curve (the zero-angle scattering intensity $I(0)$, the observed mean-square gyration radius R_{g}^2, and the Porod volume V_{P}):

$$I(0) = nV_{\mathrm{c}}^2(\Delta\rho)^2\,, \tag{32a}$$

$$R_{\mathrm{g}}^2 = R_{\mathrm{c}}^2 + \frac{\alpha}{\Delta\rho} - \frac{\beta}{(\Delta\rho)^2}\,, \tag{32b}$$

$$V_{\mathrm{P}}^{-1} = V_{\mathrm{c}}^{-1} + (\Delta\rho V_{\mathrm{c}})^{-2} \int_{V_{\mathrm{c}}} \rho_{\mathrm{f}}^2(\mathbf{r})\,\mathrm{d}\mathbf{r}\,, \tag{32c}$$

where n is the particle number density, V_{c} and R_{c} are the volume and the corresponding shape gyration radius, and $\rho_{\mathrm{f}}(\mathbf{r}) = \rho(\mathbf{r}) - \bar{\rho}$ are SLD fluctuations around its average value inside the particle. The parameters α and β in the quadratic dependence of the observed gyration radius on the inverse contrast are also defined in terms of $\rho_{\mathrm{f}}(\mathbf{r})$:

$$\alpha = V_{\mathrm{c}}^{-1} \int_{V_{\mathrm{c}}} \rho_{\mathrm{f}}(\mathbf{r})\mathbf{r}^2\,\mathrm{d}\mathbf{r}\,, \tag{33a}$$

$$\beta = V_{\mathrm{c}}^{-2} \int_{V_{\mathrm{c}}} \int_{V_{\mathrm{c}}} \rho_{\mathrm{f}}(\mathbf{r}_1)\,\rho_{\mathrm{f}}(\mathbf{r}_2)(\mathbf{r}_1\mathbf{r}_2)\,\mathrm{d}\mathbf{r}_1\,\mathrm{d}\mathbf{r}_2\,. \tag{33b}$$

The parameters α and β describe the relative distribution of 'heavy' and 'light' (in terms of scattering) components inside the particle [49, 73, 74]. For $\alpha > 0$, heavy components are located at the periphery of the particle and the light ones close to the center of mass; the situation is opposite for $\alpha < 0$. The value of the parameter $\beta \geqslant 0$ reflects the characteristic length between the centers of mass of different components within the particle. The case $\beta = 0$ corresponds to layered closed structures, such as a coated sphere. Expression (32b) may take negative values, and the quadratic form of the gyration radius in (32b) is used arbitrarily (a form of the Guinier law for homogeneous particles).

At the point $\Delta\rho = 0$, the mean SLDs of the particles and the solvent coincide and the small-angle signal disappears as $q \to 0$. In other words, it follows from (32a) that $I(0) = 0$. In this case, the corresponding solvent density is called the match point. Usually, it is expressed as a percentage of the relative volume fraction of the D-component in the solvent used to vary contrast. This means that the average particle SLD (an integral characteristic of the SLD distribution inside the particle) can be found experimentally by measuring the match point. The next step in determining the SLD integral characteristics in the particle is the analysis of the contrast dependence of gyration radius (32b); it yields the α and β values.

A special point in dependences (32) is the infinite contrast point $(\Delta\rho)^{-1} = 0$. Here, dependence (32b) intersects the R_g^2 axis at R_c^2, the point corresponding to the particle shape gyration radius, and dependence (32c) traverses the V_P^{-1} axis at the point V_c^{-1} corresponding to the inverse volume of the particle.

3.2 Taking polydispersity into account

Further development of the basic function approach in the general case of polydisperse particles was undertaken in [75]. In the case of polydisperse particles, relation (31) must be averaged over the polydispersity function:

$$I(q) = \langle I_s(q)\rangle + \langle \Delta\rho\, I_{cs}(q)\rangle + \langle (\Delta\rho)^2 I_c(q)\rangle\,. \tag{34}$$

For polydisperse particles coated with a stabilizing surfactant layer of the same thickness, the mean density $\bar{\rho}$ varies from particle to particle, which justifies the inclusion of the contrast in averaging in (34). As shown in [75], introduction of the modified contrast

$$\Delta\tilde{\rho} = \bar{\rho}_e - \rho_s\,, \tag{35}$$

where

$$\bar{\rho}_e = \frac{\langle \bar{\rho} V_c^2\rangle}{\langle V_c^2\rangle}\,, \tag{36}$$

converts (34) into expression (31) of a classical form with modified basic functions:

$$I(q) = \tilde{I}_s(q) + \Delta\tilde{\rho}\tilde{I}_{cs}(q) + (\Delta\tilde{\rho})^2\tilde{I}_c(q)\,. \tag{37}$$

The modified basic functions are defined in terms of the classical basic functions and the polydispersity function as

$$\tilde{I}_c(q) = \langle I_c(q)\rangle\,, \tag{38a}$$

$$\tilde{I}_s(q) = \langle I_s(q)\rangle + \langle (\bar{\rho} - \bar{\rho}_e)\, I_{cs}(q)\rangle + \langle (\bar{\rho} - \bar{\rho}_e)^2 I_c(q)\rangle\,, \tag{38b}$$

$$\tilde{I}_{cs}(q) = \langle I_{cs}(q)\rangle + 2\langle (\bar{\rho} - \bar{\rho}_e)\, I_c(q)\rangle\,. \tag{38c}$$

The basic function $\tilde{I}_c(q)$ is easy to interpret despite the complication. It is actually the average of 'shape scattering' over all varieties of particles present in the system.

The dependences of integral parameters on the modified contrast are different from those in a monodisperse case:

$$I(0) = n\langle V_c^2\rangle(\Delta\tilde{\rho})^2 + n\langle V_c^2\rangle D\,, \tag{39a}$$

$$\tilde{R}_g^2 = \frac{\langle V_c^2 R_c^2\rangle/\langle V_c^2\rangle + A/\Delta\tilde{\rho} - B/(\Delta\tilde{\rho})^2}{1 + D/(\Delta\tilde{\rho})^2}\,, \tag{39b}$$

$$\frac{1}{\tilde{V}_P} = \frac{\langle V_c\rangle/\langle V_c^2\rangle + E/\Delta\tilde{\rho} + F/\Delta\tilde{\rho}^2}{1 + D/\Delta\tilde{\rho}^2}\,, \tag{39c}$$

where A, B, D, E, and F are certain parameters analogous to α and β in (32). It follows from (39a) that the forward scattering intensity has a quadratic minimum at the point $\Delta\tilde{\rho} = 0$. By analogy with (32), the SLD of $\bar{\rho}_e$ may be regarded as the effective match point corresponding to this minimum. However, it is a nonzero minimum, in contrast to the zero minimum in the dependence $I(0) \sim \Delta\rho$ for a monodisperse system. In other words, the residual intensity for which the parameter D is responsible occurs at the effective match point of a polydisperse system. Also, there are essential differences from (32b, c) for the observed mean-square gyration radius and the Porod volume that tend to the respective limits $-B/D$ and F/D as $\Delta\tilde{\rho} \to 0$. In the monodisperse case, this region is usually disregarded because of weak scattering (complete compensation). Thus, on the one hand, averaging over the polydispersity function results in the loss of information; on the other hand, residual intensity at the effective match point allows thoroughly examining its vicinity to determine the integral scattering characteristics.

3.3 Taking magnetic scattering into account and the contrast variation in magnetic fluids

As shown in Ref. [75], additional magnetic scattering can be naturally introduced into the above formalism of modified basic functions. Because the scattering is independent of SLD variations in the solvent, $\tilde{I}_s(q)$ is the sole changing function:

$$\tilde{I}_s(q) \to \tilde{I}_s(q) + \langle I_M(q)\rangle\,. \tag{40}$$

We note that in this case, the form of expression (39) remains unaltered and magnetic scattering occurs at the effective match point, besides residual scattering due to polydispersity.

The first contrast variation experiments with MFs [76] were carried out in the framework of the classical approach, neglecting the effects of polydispersity and magnetic scattering. In later studies, residual intensity in the scattering minimum was interpreted as purely magnetic scattering [77]. The dependence of the zero-angle scattering intensity on the D-solvent content in the solution was calculated for the log-normal distribution over the radius of magnetic particles [78]. However, the polydispersity parameter was taken equal to zero for practical purposes (the study of magnetite/oleic acid/benzene MF).

An example of the use of the modified basic function approach [75] is presented in Fig. 7 for a low-concentration nonpolar MF containing magnetite ($\varphi_m = 0.008$) and stabilized with different monocarboxylic acids, including oleic acid (OA) and saturated myristic acid (MA) having a linear molecule (without a bend). As shown in Refs [31, 78, 80], short-chain saturated acids [lauric (C_{12}) and myristic (C_{14})] can be used to synthesize rather concentrated MFs despite the lower stabilization efficiency. Contrast variation demonstrated a significant difference between particle structures in MFs stabilized by saturated acids and classical OA. To realize contrast variation, the starting samples in D-benzene with $\varphi_m = 0.08$ were diluted 10-fold with different mixtures of H- and D-components of the solvent. This allowed varying the volume fraction of the D-component in the range 10 – 100% without the loss of sample identity. Figure 7 shows how the curves change with variation of the solvent deuteration degree.

The results of the analysis of the integral parameters (zero-angle scattering intensity and the observed mean-square radius of gyration) by the above procedure are shown in Fig. 8. The Guinier analysis of the curves presented in Fig. 7 was followed by the calculation of $I(0)$ as a function of the D-component volume fraction in the solvent (Fig. 8a). Parabolic dependence minima gave effective match points expressed as a percentage of the D-component content in the solvent that were further used to determine modified contrast (35). A shift of the match point toward lower values (34.2% for MA vs 63.0% for OA) suggested an increase in the volume fraction of surfactants in MF particles. This fact can be accounted for by a decrease in the mean size of the MA-stabilized magnetite particles,

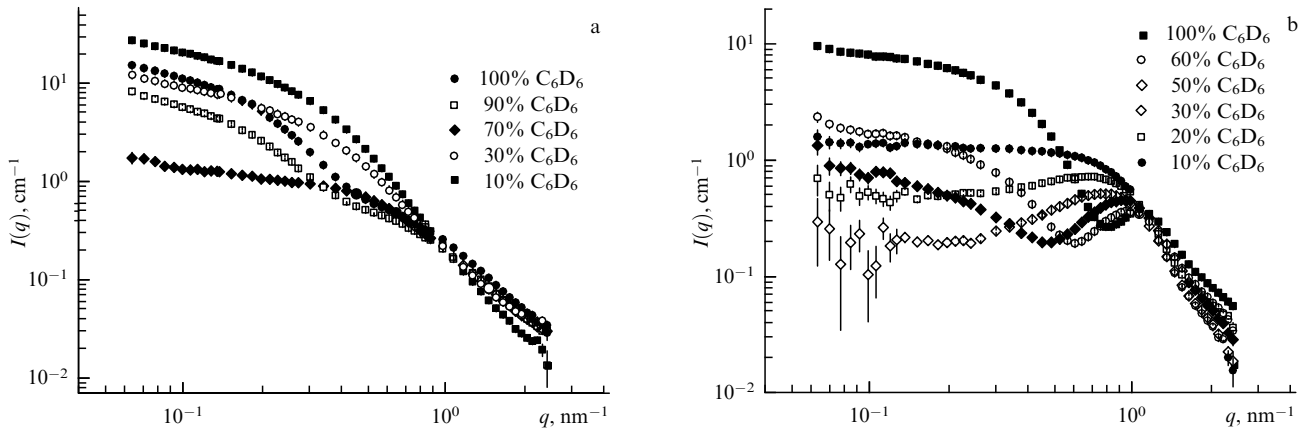

Figure 7. SANS curves obtained by contrast variation in nonpolar organic MFs with magnetite ($\varphi_m = 0.008$) stabilized by (a) oleic and (b) myristic acids in benzene (GKSS). For the sake of illustration, only a part of the contrasts is shown. Sample designations specify the D-component percent content in the solvent.

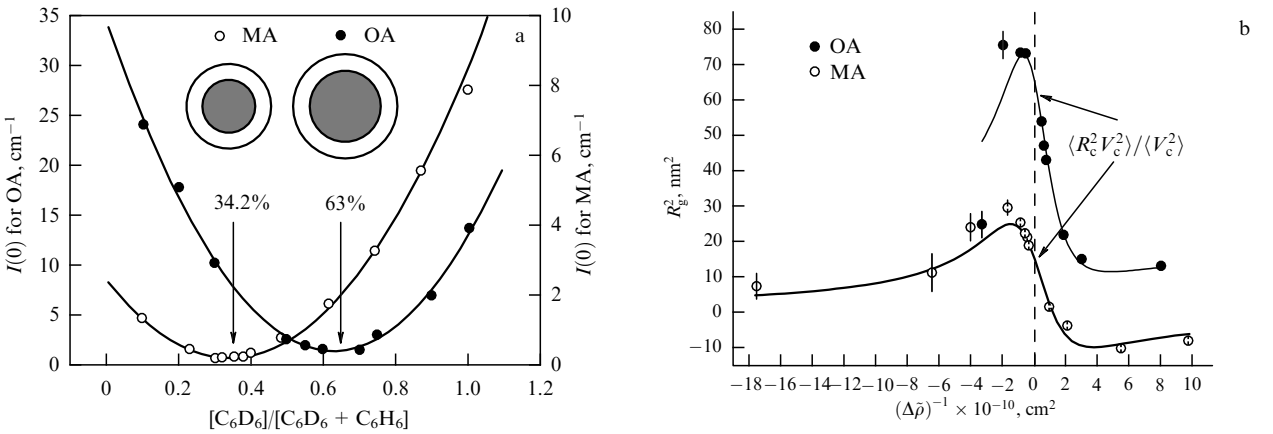

Figure 8. Changes in the integral parameters of the SANS curve shown in Fig. 7 upon contrast variation in magnetite-containing MFs stabilized with oleic (OA) and myristic (MA) acids in benzene. (a) Forward scattering intensity as a function of the D-component relative volume fraction in the solvent. Arrows indicate the effective match points. The diagram explains the changes in the relative surfactant content in a particle upon substitution of OA by MA for MF synthesis. (b) The observed mean-square radius of gyration as a function of the inverse modified contrast. Results of fitting (39b) for the OA sample: $\langle V_c^2 R_c^2\rangle/\langle V_c^2\rangle = 64.4 \pm 0.7$ nm^2, $A = (-22.3 \pm 0.7) \times 10^{-3}$, $B = (-5.7 \pm 0.3) \times 10^5$ cm^{-2}, $D = 2.87 \times 10^{19}$ cm^{-4}; for the MA sample: $\langle V_c^2 R_c^2\rangle/\langle V_c^2\rangle = 15.1 \pm 0.1$ nm^2, $A = (-1.34 \pm 0.01) \times 10^{-3}$, $B = (-1.4 \pm 0.4) \times 10^5$ cm^{-2}, $D = 1.81 \times 10^{19}$ cm^{-4} [in both cases, the parameter D was first derived from (39a)].

while the surfactant coating thickness remained roughly identical in both cases (Fig. 8a). Thus, the overall particle size decreases, as is confirmed by the analysis (Fig. 8b) of the observed mean-square radius of gyration as a function of the inverse modified contrast with the relevant fitting according to (39b): the averaged mean-square radius of gyration of the particles $\langle V_c^2 R_c^2\rangle/\langle V_c^2\rangle$ changes from 64.4 to 15.1 nm^2. In the spherical approximation, it corresponds to the total mean-square radii 10.4 and 5.1 nm.

Basic functions can be found by minimizing the functional [81]

$$\chi^2 = \frac{1}{N-3}\sum_k \frac{\left[I_k(q) - \tilde{I}_s(q) - \Delta\rho_k \tilde{I}_{cs}(q) - (\Delta\rho_k)^2 \tilde{I}_c(q)\right]^2}{\sigma_k^2(q)}, \tag{41}$$

known from applications of the classical approach for monodisperse systems. Here, $I_k(q)$ and $\sigma_k(q)$ are the experimental scattering intensity and its error at a point q measured at the kth contrast, and N is the number of contrasts in the experiment. For the verification of the solutions, the functions $\tilde{I}_c(q)$ are compared with the scattering in the vicinity of match points (Fig. 9a). The two parameters perfectly coincide, suggesting the high reliability of the solution. The basic functions $\tilde{I}_c(q)$ obtained for two samples are compared in Fig. 9b. An important aspect of the use of the basic function approach for MFs is the subsequent comparison of $\tilde{I}_c(q)$ with the scattering on pure magnetite in an H-solvent. The function $\tilde{I}_c(q)$ corresponds to shape scattering on the particles including their shells, whereas scattering on magnetite reflects scattering on the central 'spheres' of complex particles. The inset in Fig. 9b compares radial distribution functions obtained from the respective curves by the indirect Fourier transformation. To account for the particle structure, these functions are shifted relative to each other by the surfactant shell thickness, which allows estimating this thickness from the contrast variation data. The figure shows that the surfactant layer thickness for two acids is practically identical (roughly 1.5 nm), in agreement with the presence of the bend in the OA molecule that decreases its effective length.

One more example of the analysis of the basic function $\tilde{I}_c(q)$ for an MF with fractal aggregates [82, 83] is shown in Fig. 10 (aqueous MF stabilized by substitution of sodium

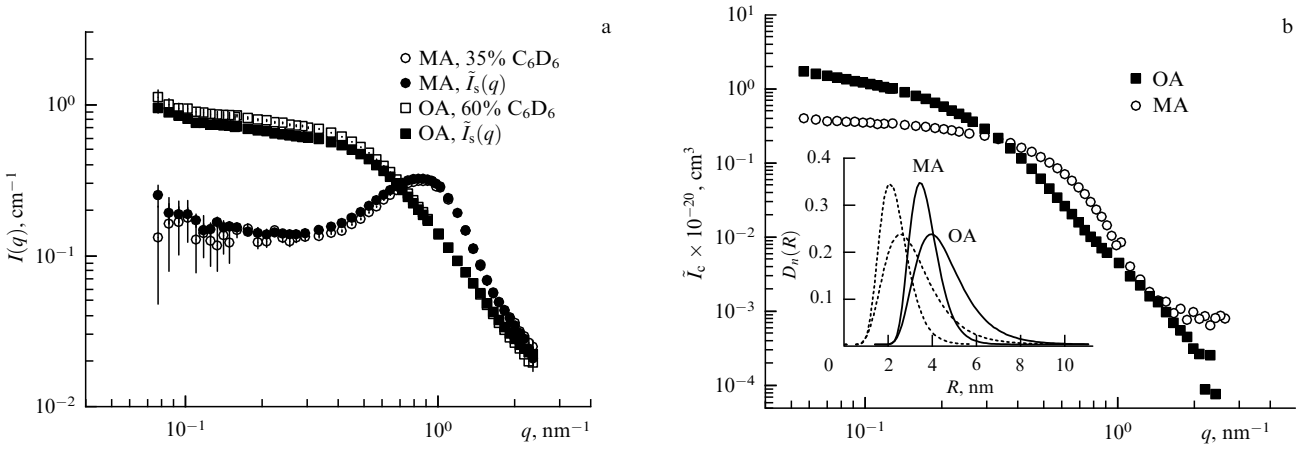

Figure 9. (a, b) Basic functions $\tilde{I}_s(q)$ and $\tilde{I}_c(q)$ derived from the curves in Fig. 7. (a) Comparison of $\tilde{I}_s(q)$ with the SANS curves measured in the vicinity of effective match points. (b) The inset compares the radial distribution functions derived from $\tilde{I}_c(q)$ (solid curves) with scattering data for samples containing no D-component (dotted curves). The surfactant shell thickness estimated from the shift of different distribution types is identical for both samples ($\sim$ 1.4 nm).

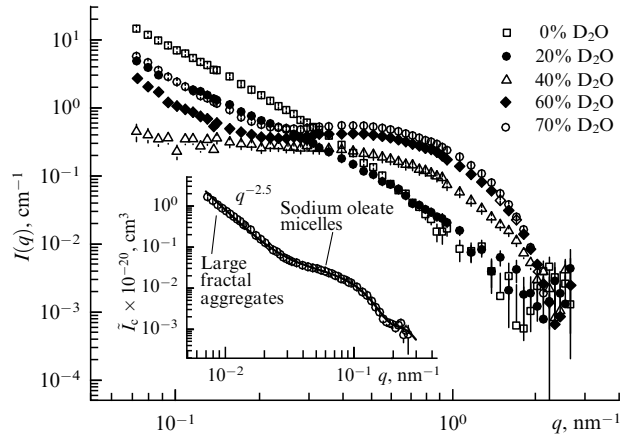

Figure 10. Changes in SANS curves (GKSS) upon contrast variation in an aqueous MF stabilized by substitution of polyethylene glycol for sodium oleate at different D_2O levels in the solvent. For the sake of illustration, only part of the contrasts is shown. The inset shows the basic function $\tilde{I}_c(q)$ with distinguished scattering regimes.

oleate $C_{17}H_{33}COONa$ by biocompatible polyethylene glycol $HO-CH_2-(CH_2-O-CH_2-)_n-CH_2-OH$ with the molecular mass $M_w = 1000$). At small q, the fractal nature of scattering (15) becomes apparent for clusters whose size is beyond the resolution of the experimental setup; this makes the Guinier analysis impracticable. In this case, as is shown in Ref. [75], it is possible to use an arbitrary effective match point in (35). Despite the resulting complication of the expressions for basic functions, the function $\tilde{I}_c(q)$ remains invariant with respect to the choice of $\bar{\rho}_e$; this means that with any choice, $\tilde{I}_c(q)$ represents 'shape scattering.' Moreover, according to (37), the function $\tilde{I}_s(q)$ describes residual scattering at an effective match point and can be used to verify solutions in analogy with the preceding example. As shown in the inset of Fig. 10, there are two scattering modes for $\tilde{I}_c(q)$: on large fractal clusters (dimension 2.5, size > 120 nm) and on micelles of sodium oleate (gyration radius 1.6 nm) remaining unadsorbed in the solution. Other examples of the analysis of contrast variation data obtained on complex cluster structures in aqueous MF can be found in Refs [18, 84, 85].

Scattering on mono- and polydisperse homogeneous magnetic particles can also be interpreted using the modified basic function method [75]. In particular, this can be seen in the example of an MF with electrostatic stabilization of maghemite in water and a rather small contribution of stabilizing ion shells to the scattering [86]. The experiment was carried out under conditions of compensation of the Coulomb (addition of a salt) and magnetic (dilution) interactions. The difference between the observed 'nuclear' (atomic) and magnetic sizes (10.1 vs 7.2 nm for the experimental mean-square radius of gyration) was interpreted as a result of different correlation lengths of nuclear and magnetic scattering due to the strong residual van der Waals interaction (nonuniform distribution of the adsorbed charge over the maghemite surface).

4. The structure of nonmagnetized magnetic fluids

4.1 Weakly interacting particles

The structural parameters of MF particles can be determined by directly fitting (23) to experimental data. For MFs with isolated polydisperse particles (see Fig. 1), $D_n(R)$ is usually a log-normal distribution:

$$D_n(R) = \frac{1}{\sqrt{2\pi}\,SR} \exp\left[-\frac{\ln^2(R/R_0)}{2S^2}\right], \tag{42}$$

where R_0 and S characterize the mean radius and the variance of the distribution. The use of nuclear (28) and magnetic (29) scattering form factors for total intensity (27) in a low-concentrated MF in the absence of an external magnetic field yields the model function

$$\begin{aligned} I(q) = {} & \left(\frac{4}{3}\right)^2 \pi^2 n \int \Big[(\rho_0 - \rho_1) R^3 \Phi(qR) \\ & + (\rho_1 - \rho_s)(R+h)^3 \Phi\big(q(R+h)\big)\Big]^2 D_n(R)\,\mathrm{d}R \\ & + \frac{2^5}{3^3}\pi^2 n \rho_m^2 \int (R-\delta)^6 \Phi^2\big(q(R-\delta)\big) D_n(R)\,\mathrm{d}R\,. \end{aligned} \tag{43}$$

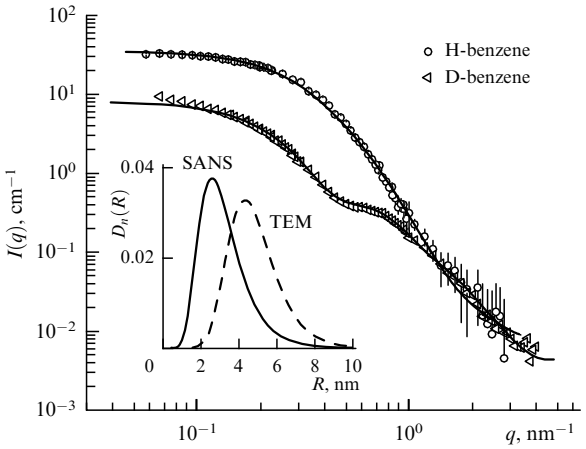

Figure 11. Fitting the obtained SANS curves for the MF in H- (44) and D- (43) solvents (benzene) (JINR and BNC). The parameters of $D_n(R)$ are varied in H-benzene and fixed in D-benzene, where $\delta = 0$ and the parameters h and ρ_1 are varied. The inset compares the functions $D_n(R)$ obtained by SANS and TEM at the Centre of Fundamental and Advanced Technical Research, Romanian Academy of Sciences (CFATR).

In the general case, formula (43) has a rather large number of free parameters. The variable structural parameters R_0, S, h, δ, and ρ_1 should be supplemented by the parameter n (that may contain an error in determining the concentration by other methods and an error in reducing the SANS curve to an absolute value) and the residual background. For a reliable fitting of (43) to experimental data, some parameters need to be fixed using a priori information. For example, the authors of Ref. [87] took the parameters of the function $D_n(R)$ for a D-benzene-based MF (magnetite coated with a single layer of oleic acid) from the results of electron microscopic analysis and assumed δ to be zero. Such a simplification ensured a stable fitting (Fig. 11) from which h and ρ_1 could be determined. The deuterated base was used in the MF to have the maximum contribution (according to Fig. 6) from the surfactant shell. The values for 1% MF ($h = 1.85 \pm 0.05$ nm and $\rho_1 = (0.26 \pm 0.15) \times 10^{10}$ cm^{-2}) thus obtained proved to be close to the expected ones. The deviation of ρ_1 from the SLD of the liquid surfactant ($\rho_1 = 0.077 \times 10^{10}$ cm^{-2}) may be interpreted as a result of penetration of the deuterated solvent into the shell. However, the near-zero value of ρ_1 precludes precise estimation of the degree of such penetration. Nevertheless, the attained precision of the ρ_1 value (determined by the accuracy of measurements by the SANS method) allows concluding that the solvent content in the shell does not exceed 5%.

The contribution of the shell may be neglected when using H-solvents. In this case, the scattering curve is smoothed (see Fig. 11). Interestingly [30, 88], the fitting is completely insensitive to the magnetic term (for a magnetite-containing MF). The agreement is improved when this term is totally disregarded, i.e., when formula (43) is reduced to

$$I(q) \approx \left(\frac{4}{3}\right)^2 \pi^2 n(\rho_0 - \rho_s)^2 \int R^6 \Phi^2(qR) D_n(R)\,\mathrm{d}R\,. \qquad (44)$$

It can be concluded that magnetic scattering in the case of H-solvents is negligibly small compared with the nuclear one. This inference is confirmed by polarized neutron scattering data (see Section 5). As shown below, this is due to marked magnetic correlations even in the low-concentration MF responsible for the general impairment of magnetic scattering within the q-range being used. This suggests that magnetic scattering is taken into account in (43) inaccurately. When the magnetic term is discarded, marked discrepancies between theoretical and experimental curves are apparent only for sufficiently small q (see Fig. 11), where the influence of the magnetic component remains significant.

Expression (44) permits determining the parameters of the function $D_n(R)$ for magnetite from the SANS curves in H-solvents. An example of the respective adjustment is presented in Fig. 11 for a benzene-based MF of the same type [89]. The SANS technique yields a smaller nanoparticle size in the MF than transmission electron microscopy (TEM), the difference being almost twofold for the sizes shown in the inset of Fig. 11. This feature was also noticed in Refs [45, 90]. The cause behind the overestimation of nanoparticle size in TEM may be the different sensitivity of the two methods to the size range being investigated. Also, the procedure of preparing samples for TEM studies may give rise to different aggregates, effectively altering the distribution of isolated (unaggregated) particles included in the analysis. It is argued in Ref. [90] that the cause of the discrepancy is the deviation of the shape of magnetic nanoparticles from spherical ones.

One more well-known method for the determination of $D_n(R)$ is based on an analysis of the magnetization curve (magnetic granulometry) containing information on the nanoparticle magnetic size distribution. On the whole, this method gives even smaller mean sizes than SANS [88, 90]. On the one hand, it suggests the existence of the aforementioned magnetic layer on the particle surface. Another important circumstance for SANS may be the effect of structure factors determined by different atomic and magnetic correlation lengths and insignificant nonequilibrium aggregation of particles, as discussed in Sections 4.2, 4.3.

It follows from the above that the use of the data for $D_n(R)$ obtained by other methods when fitting expression (43) and taking magnetic scattering into account is not quite correct. This inference is confirmed by the fact that neglecting the magnetic term and additionally varying the $D_n(R)$ parameters for the scattering curves on an MF in D-bases gives results (see Fig. 11) in excellent agreement with the data for MFs in H-bases and the polarized neutron scattering data [91].

An example of the direct treatment of the SANS curves for a series of MFs is presented in Fig. 12, demonstrating the influence of oleic acid substitution by saturated acids with straight carbon chains of different lengths, such as lauric (LA), myristic (MA), palmitic (PA), and stearic (SA) acids, for magnetite stabilization in decalin. As shown in [31, 34, 92], an important difference from stabilization by OA is the presence of a finite size distribution function for magnetite having a significantly smaller mean size and width. It is especially well apparent in scattering on H-solvents (Fig. 12a). Interestingly, the corresponding $D_n(R)$ functions are very similar despite the use of the dependence of the effective MF stabilization on the carbon chain length of the saturated acid. At the same time, the SANS curves on an MF in a D-solvent (Fig. 12b) suggest different scattering modulation, depending on the carbon chain length; this reflects the difference in the surfactant coating thickness around magnetite nanoparticles. The results of fitting the scattering curves shown in Fig. 12 are summarized in Table 2.

Thus, a combination of SANS measurements for MF in H- and D-solvents neglecting analysis of the magnetic

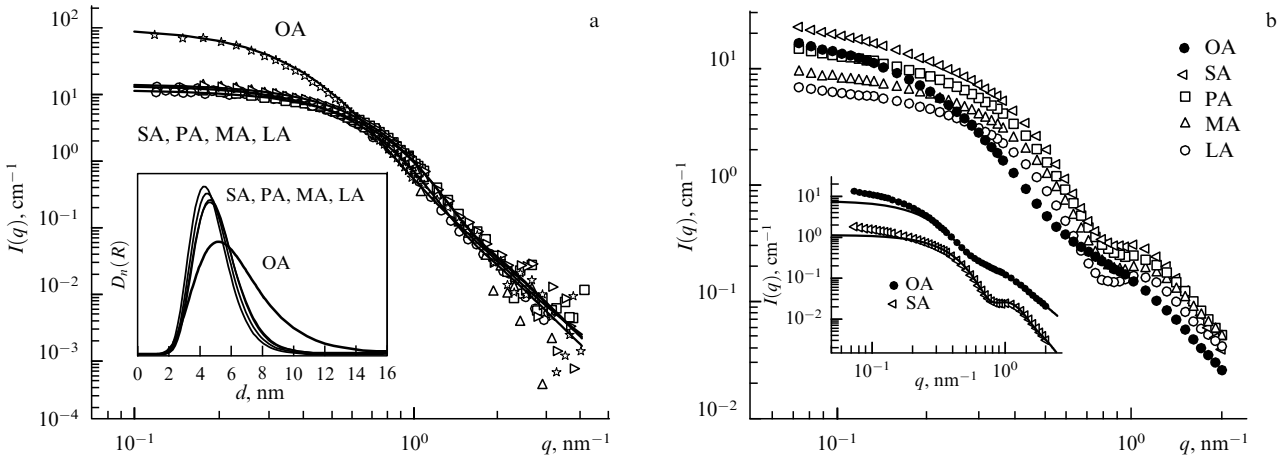

Figure 12. SANS curves (BNC, GKSS) for MF in H-decalin (a) and 90% D-decalin (b) reduced to the same concentration. (a) $\varphi_m = 1.5\%$; the lines show the results of fitting by model (44); the inset shows the corresponding magnetite distribution functions. (b) $\varphi_m = 0.6\%$; the inset shows examples of curve fitting by model (43); the values of the curve for SA are divided by 10 for the purpose of illustration.

Table 2. The parameters R_0 and S of distribution function (42) of magnetite stabilized with different acids in decalin and the thickness h of the surfactant shell obtained by directly fitting the SANS curves presented in Fig. 12. The relative errors of all values do not exceed 5%.

Surfactant	R_0, nm	S	h, nm	R_{dif}, nm*
OA	3.40	0.38	1.40	4.3
SA	2.55	0.28	1.85	2.3
PA	2.48	0.28	1.55	2.6
MA	2.65	0.28	1.35	2.5
LA	2.51	0.28	1.25	2.8

* For comparison, effective radii of magnetite crystals R_{dif} in MF are presented (obtained by analysis of the broadening of synchrotron radiation diffraction peaks at the Kurchatov Centre of Synchrotron Radiation and Nanotechnologies, KCSR&NT).

scattering component provides a tool for rather accurate and rapid determination of the parameters of MF particles. First, measurements in the H-solvent are used to determine the parameters of $D_n(R)$; thereafter, these parameters are used to treat the curves for the D-solvent and thereby to find h and ρ_1. Such treatment helps estimate the influence of different conditions on the internal structure of MFs without more sophisticated contrast variation experiments or experiments in a magnetic field with the use of polarized neutrons.

Direct simulation of scattering curves was also used in the analysis of the structure of nonmagnetized magnetite-based MFs in nonmagnetized media (single stabilization) [93–95] and of aqueous dispersions (double stabilization) of magnetite [96, 97] and ferrites [98]. An interesting additional method was proposed for the interpretation of scattering curves for an organic MF with MnZn-type ferrites having a low Curie temperature ($T_C = 340$ K) [99]. The relatively low heating of the MF allowed eliminating the magnetic constituent from the scattering curve. However, the 'nuclear' (atomic) MF structure may also change at increased temperatures due to the temperature dependence of surfactant adsorption on the surface of magnetic materials; this may lead to the disturbance of stability and additional aggregation [30].

In addition to magnetization analysis and electron microscopy, the SANS technique is also used in combination with X-ray (synchrotron) diffraction on magnetic crystals dispersed in MFs. The analysis of the broadening of diffraction peaks (see, e.g., [100–107]) gives a rough idea of the mean crystallite (magnetic nanoparticle) size; these data are compared with $D_n(R)$ estimates from SANS studies. Table 2 contains comparative results of synchrotron diffraction for the effective radius of magnetite crystals stabilized by different acids in decalin [107]. A decrease in this radius upon substitution by saturated acids confirms the results of SANS and proves that the effect is unrelated to different particle aggregations (at which the mean magnetite crystal size would remain unaltered).

The magnetic size of nanoparticles can be determined by the aforementioned analysis of static magnetization curves (magnetic granulometry) [90, 108, 109] and by Mössbauer spectroscopy [65, 66] or muon spectroscopy (muon-spin relaxation) [110–112]. Experiments with the use of small-angle X-ray scattering (SAXS) are very similar to neutron experiments in H-solvents. In the case of SAXS, the magnetic constituent of scattering is absent as such. Moreover, the scattering largely occurs on magnetic nanoparticles due to the small contrast between electron densities of the surfactant shell and the solvent; for this reason, SAXS can be used in these systems only to determine the parameters of $D_n(R)$. Modern SANS spectrometers can measure smaller q values than laboratory SAXS units and thereby provide more exact estimates of the $D_n(R)$ parameters. Moreover, calibration methods in SANS, unlike SAXS, permit simply and accurately reducing scattering curves to absolute scattering cross section values. On the other hand, the use of synchrotron sources in SAXS experiments allows covering the same q range as in SANS in much less time. SAXS was used to determine MF characteristics in Refs [93, 105, 107, 113–115].

If particles begin to aggregate in an MF originally consisting of dispersed isolated particles (see Fig. 1), the main changes in the scattering curves fall within the region of small q values. This is the so-called structure factor effect (see Section 4.3). At sufficiently large q values, when this effect is either small or nonexistent, the above simulation can be undertaken. It was used for different MF clusters in Refs [30, 45, 116, 117].

4.2 Interacting particles

Investigations of the effect of the interaction between MF particles using SANS encounter two fundamental difficulties.

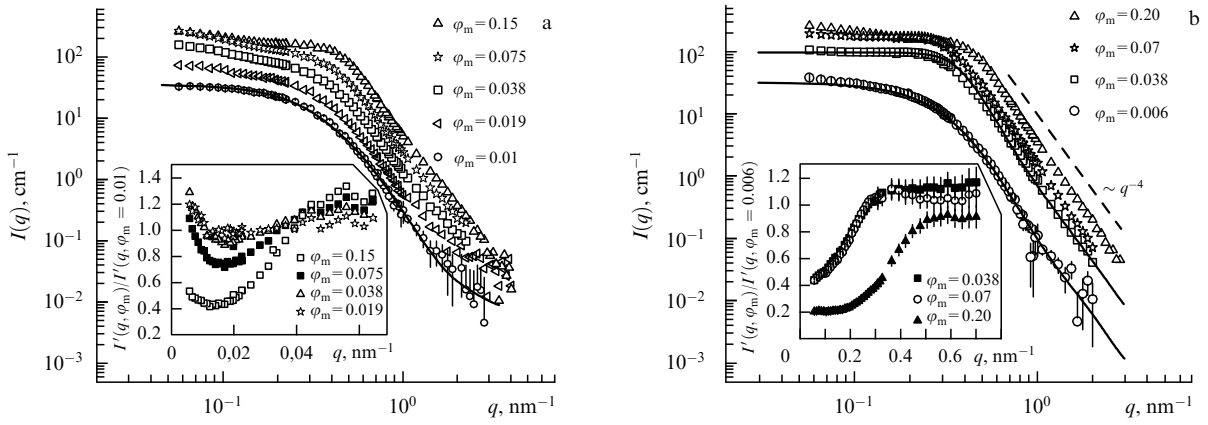

Figure 13. Experimental SANS curves (BNC) at different magnetite volume fractions for (a) benzene and (b) pentanol-based MFs. Solid lines are simulated dependences at minimal φ_m according to (44) with the use of distribution (42). The insets show the effective 'nuclear' structure factors at increased concentrations.

First, the particles are strongly polydisperse. Second, the magnetic interaction depends on their mutual orientation and is not isotropic. A rigorous mathematical description of these two characteristics is very difficult to propose because the effect of the interaction cannot be factored, in contrast to the monodisperse particles with the isotropic interaction described in Section 2.2.3. Researchers usually confine themselves to qualitative estimates of this effect based on simplifying assumptions. For example, in the first approximation (in the absence of an external magnetic field), it is possible to write [118]

$$I(q) \approx nF_{\mathrm{N}}^2(q)\, S_{\mathrm{N}}(q) + \frac{2}{3}\, nF_{\mathrm{M}}^2(q)\, S_{\mathrm{M}}(q)\,, \tag{45}$$

where $S_{\mathrm{N}}(q)$ and $S_{\mathrm{M}}(q)$ are effective structure factors corresponding to correlations between positions of the particles ('nuclear' structure factor) and between their magnetic moments (magnetic structure factor). In (45), $S_{\mathrm{N}}(q)$ and $S_{\mathrm{M}}(q)$ are assumed to be independent, the particles low-polydisperse, and the factor $S_{\mathrm{M}}(q)$ isotropic.

As shown in Section 4.1, magnetic scattering on an H-solvent-based MF may be neglected in order to reduce the analysis to $S_{\mathrm{N}}(q)$. For this, the scattering curve measured at a low particle concentration, i.e., corresponding to the form factor $F_{\mathrm{N}}^2(q)$, is used. The ratio of the curve measured at a higher concentration to the designated curve with simultaneous calibration for the particle concentration gives the effective structure factor $S_{\mathrm{N}}(q)$ in formula (45). This procedure is illustrated in Fig. 13 for two types of MFs on organic bases [30, 89]. The effective structure factors are smoothed compared with those in monodisperse particle systems. In the first case (Fig. 13a), a single layer of oleic acid was used to stabilize magnetite in benzene. The character of the effective structure factor suggests the presence of an attraction component in the interparticle interaction potential, as follows from the increase of $S_{\mathrm{N}}(q)$ at small q. In the second case (Fig. 13b), when magnetite is dispersed in pentanol with a double layer of oleic and dodecylbenzene sulphonic (DBSA) acids, $S_{\mathrm{N}}(q)$ is qualitatively different from the effective structure factor in the first case; specifically, there is no increase at the origin of the curves and $S_{\mathrm{N}}(q)$ significantly decreases as the particle concentration increases. Thus, the qualitative analysis demonstrates the complete screening of attraction in a doubly stabilized MF.

The observed difference in the character of the interaction accounts for the considerable difference between the magnetorheologic properties of the two types of MFs [29, 119]. In concentrated pentanol-based MFs, the magnetoviscous effect (increased viscosity under the action of an external magnetic field) directly related to the formation of chain-like aggregates is practically absent. The obtained data on particle interactions confirm the importance of a strong attraction component in the interaction potential (like the one present in a nonpolar MF) for the formation of such aggregates. However, the thickening surfactant layer screens the attraction and thereby hampers aggregation. High-concentration MFs with a low magnetoviscous effect are used, for example, in high-vacuum gears and bearings where any aggregate formation is undesirable. Similarly, a change in the interaction pattern occurs in aqueous ionic MFs upon variation of the pH and ionic strength of the solution [43, 118, 120–123]. Such variation can be used to control the interaction parameter in the system. Reversible (with respect to the applied field) phase separation occurs at a certain critical value of the stability parameter in a magnetic field [124–126]. Optical microscopy reveals isolated needle-like droplets oriented along the field, which disappear after it is removed. Here, SANS is used to describe the character of the interaction that serves as a basis to construct the phase diagram for such systems.

Possibilities for the exact description of the effective structure factor in SANS curves for MFs based on an H-solvent are considered in Ref. [30]. Integration in the form [45]

$$I(q) \approx n \int D_n(R)\, F_{\mathrm{N}}^2(qR)\, S_{\mathrm{N}}(qR)\, \mathrm{d}R\,, \tag{46}$$

where $S_{\mathrm{N}}(qR)$ is the structure factor corresponding to monodisperse particles with radius R, is known as the local-polydisperse approximation [51]. This approximation actually meets the requirement that a distinguished particle must be largely surrounded by particles of a similar size. Realization of this model representation in real systems encounters difficulty. Nevertheless, it is frequently used for qualitative estimates of the particle interaction radius due to the simplicity of fitting (46) to experimental data. For practically noninteracting particles (e.g., in a doubly stabilized pentanol-based MF), it is possible to use the Percus–Yevick approximation in the hard-sphere model for $S_{\mathrm{N}}(qR)$. The exact

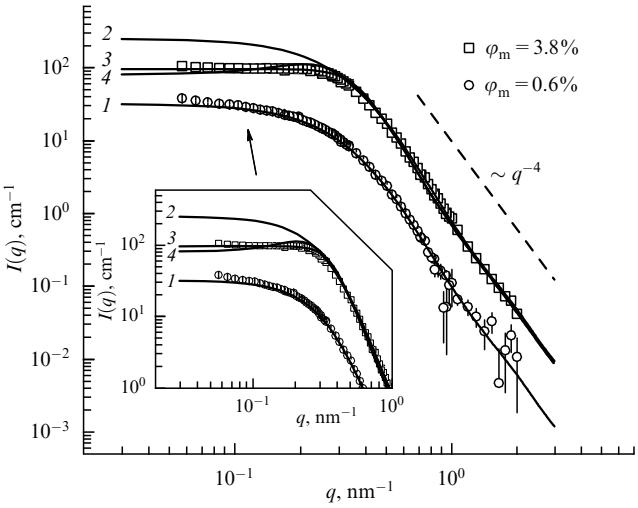

Figure 14. Approximation of experimental SANS data (squares and circles) for pentanol-based MFs by different models: curves *1*, *2* — expression (44) with the use of distribution (42) for the respective concentration; *3* — fitting based on the Vrij formalism [127]; *4* — fitting according to local-polydisperse approximation (46) with the use of the structure factor of rigid spheres. The dashed curve corresponds to the Porod power law.

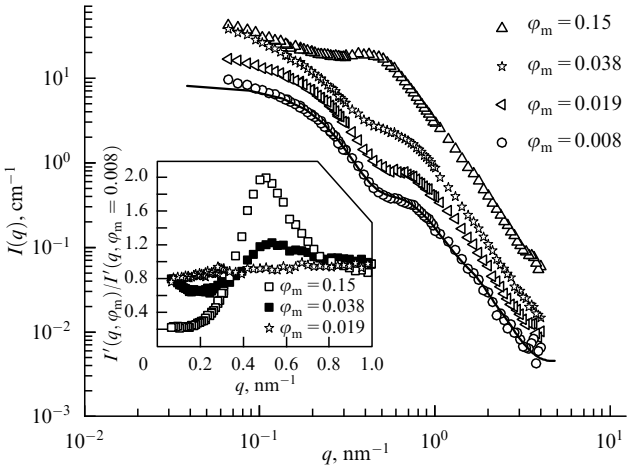

Figure 15. Experimental SANS curves (symbols) (BNC) at different magnetite volume fractions for an MF in D-benzene. The line is the model curve at minimal φ_m according to (43) with the use of distribution (42). The inset shows effective nuclear-magnetic structure factors at increased concentrations.

account of polydispersity in the description of scattering curves for interacting particles is possible only for a limited number of simple model potentials. The simplest models of noninteracting spheres in the Percus–Yevick approximation use the Vrij formalism [127, 128], in which scattering is represented as a rather large number of averagings over $D_n(R)$ for certain special functions. Despite cumbersome calculations, computation of the scattering curve and its fitting to experimental data encounter no serious difficulties in this approach.

Both approaches (the local polydisperse approximation and the Vrij formalism for a hard-sphere system) were compared [30] in the description of scattering curves (Fig. 14) for the aforementioned pentanol-based MF. It was shown that the hard-sphere approximation is applicable only at low concentrations ($\varphi_m < 6\%$). At higher concentrations, the structure factor is 'softened,' probably because surfactant shells of different particles overlap as they come closer together [30]. In this case, it is difficult to determine the volume fraction of interacting particles. The volume fraction of rigid particles used for normalization is overestimated, which accounts for the aforementioned 'softening.' Comparison of these two approaches in the description of a SANS curve for $\varphi_m = 3.4\%$ explicitly shows the advantages of the Vrij formalism (see Fig. 14). The interaction radius (radius of rigid spheres) was varied in the form of $R + h$ by changing the surfactant shell thickness. The value $h \approx 2.3$ nm thus found is significantly smaller than the total length of all surfactants used to form a double layer ($\approx 2 \times 1.8$ nm $= 3.6$ nm). This suggests strong overlapping of surfactant sublayers in the case of double stabilization.

The contribution of magnetic scattering is essential in D-solvents; therefore [according to (45)], the double effect of 'nuclear' and magnetic structure factors must be considered. Moreover, $S_N(q)$ and $S_M(q)$ begin to correlate with each other at sufficiently high concentrations, and expression (45) becomes incorrect. In the treatment of SANS data for a magnetite-containing MF stabilized with lauric acid [90] and co-polymers (45), it was assumed that $S_N(q) = S_M(q)$ and the local polydisperse approximation (46) was used. Also, there is evidence that these structure factors are different [89], as is illustrated by Fig. 15, which shows effective structure factors obtained for a D-benzene-based MF containing magnetite. There is a well-apparent difference from the case of H-benzene (Fig. 13a). It seems possible to determine the structure factor $S_M(q)$ in (45) by using the $S_N(q)$ factor known from scattering on H-solutions. However, expression (45) does not take polydispersity into account, and cannot therefore be used for exact quantitative estimation.

Both structure factors ('nuclear' and magnetic) become anisotropic in an external magnetic field. Scattering anisotropy is observed in H-solutions (i.e., for the nuclear component of scattering) in the absence of chain structures [44, 129, 130], which suggests anisotropy in the short-range order of an MF. The situation is much more complicated in D-solutions because magnetic scattering in a magnetic field is anisotropic by virtue of the prevailing orientation of the particle magnetic moments [see expression (2)]. As a result, it is extremely difficult to take the correlation between the magnetic moments (the magnetic structure factor) into account. An additional difficulty for solutions of either type can arise in the case of formation of chain-like aggregates in sufficiently concentrated MFs due to the prevailing orientation of magnetic moments. Such aggregates are oriented along the field and make an additional contribution to the anisotropy of both the nuclear and the magnetic components of scattering. Finally, polydispersity has a marked effect on the character of the particle–particle interaction in an external magnetic field. The problem of describing the two-dimensional structure factor integrating 'nuclear' (atomic) and magnetic correlations for polydisperse MFs awaits solution. Theoretical calculations of such factors for simplified model systems are reported in Refs [131–135].

4.3 Cluster formation

The SANS method is highly sensitive to cluster formation in solutions. When monodisperse particles congregate into a cluster, the scattering intensity (as in the case of interacting monodisperse particles) contains a structure factor corre-

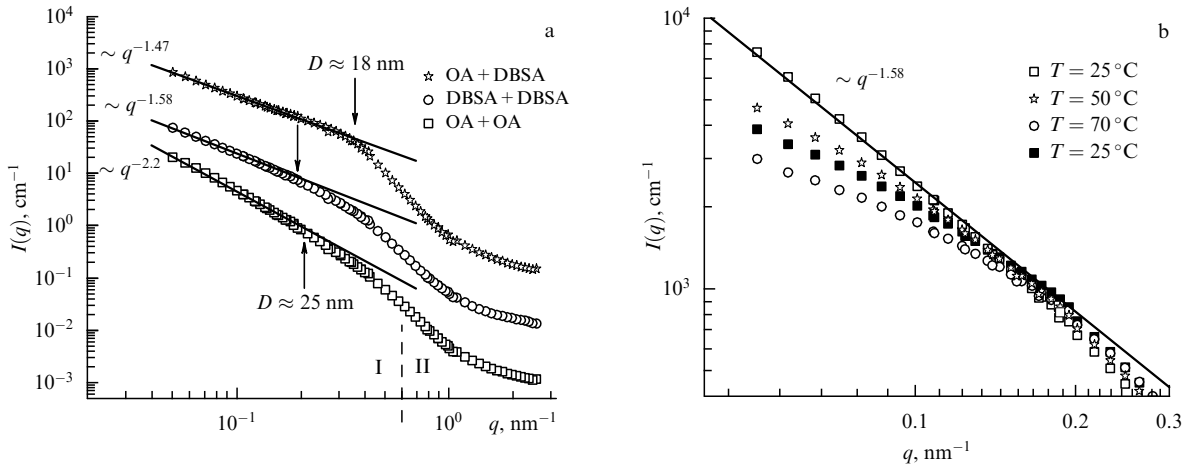

Figure 16. (a) Experimental SANS curves (symbols) (GKSS) for light water-based MFs with different surfactant combinations in a double stabilizing layer. Solid curves are power-law dependences corresponding to scattering on fractal clusters. Arrows indicate points on the scattering curves at which the power-law dependences are broken. These points are used to estimate the size of structural units in the clusters. (b) Temperature-dependent changes of the scattering curve on a DBSA + DBSA sample. The figure shows the range of q within which noticeable changes occur. After an increase in temperature to 70 °C, it decreases to room values.

sponding to correlations between monomer positions inside the cluster. If the cluster has a chain structure, nuclear scattering on it in the corresponding q interval is described by power-law dependence (15) with the exponent $\alpha = 1$ (see Table 1). The same expression but with an exponent $1 < \alpha < 3$ is used to describe scattering on a fractal cluster (see Table 1). If particles are densely packed in a cluster, the scattering curve is described by the form factor of the cluster itself. The analysis of this curve is identical to the analysis of scattering on separate particles (see Section 4.1), except that the cluster structure cannot be described by a simple 'sphere-shell' model. The power-law dependences of SANS in the form of (15) frequently occur in H-fluids, where the surfactant contribution is absent and magnetic scattering can be neglected. Examples of such dependences presented in Fig. 10 are supplemented by examples (Fig. 16) for demagnetized aqueous MFs with double stabilization based on various surfactant combinations [30]. The interval $q < 0.5$ nm^{-1} within which dependence (15) is fulfilled corresponds, in conformity with (7), to sizes over 10 nm (level I). On the double logarithmic scale, this dependence is a linear function with the proportionality coefficient $-\alpha$. The values of this parameter correspond to scattering on fractal clusters (see Table 1). In agreement with the minimal recorded value of q (0.05 nm^{-1}), the cluster size, in accordance with (7), is larger than 120 nm. Scattering at $q > 0.5$ nm^{-1} determines level II and corresponds to the structural units composing the cluster. Points on the q axis where deviation from the power law occurs with increasing q (indicated by the arrows in Fig. 16a) correspond to the characteristic size of these structural units, which depends on the nature of the sample and falls within 18 and 25 nm or is greater than the size of individual magnetite particles dispersed in nonpolar and polar organic media (see Figs 11 and 12). As shown in Refs [30, 136, 137], the behavior of the curves at level II for such MFs cannot be described by scattering on a system of polydisperse homogeneous spheres with the log-normal distribution over radii of form (42), as in the case of MFs with isolated particles (see Figs 11–13). Both factors allow concluding that fractal clusters in MFs arise from small primary aggregates (after a certain degree of condensation during preparation). An interesting observation reported in Refs [30, 33] is the temperature dependence of SANS. It turns out that level I is sensitive to an increase in temperature (Fig. 16b); namely, the fractal dimension of clusters decreases due to their disintegration. The behavior of the curves at level II remains practically unaltered. As the temperature then decreases to a room value, SANS increases again at level I, suggesting renewed cluster growth. It can be concluded that primary aggregates in aqueous MFs are rather stable, while clusters arising from them are destroyed at an increased temperature, although they can start forming again.

Examples of a similar analysis of power-law dependences of SANS for chain-like aggregates in an MF are presented in Ref. [116]. Lamellar (flat and disk-like) structures with $\alpha = 2$ have been found in Refs [116, 138].

Correlation in the orientation of magnetic moments inside a cluster is a more intricate question. If all the particles in a cluster are supposed to remain independent in terms of magnetization, then $S_{\mathrm{M}}(q) = 1$ in (45). Another limit situation corresponds to the complete ordering of magnetic moments in a cluster. In this case, the atomic and magnetic sizes of the cluster coincide and $S_{\mathrm{M}}(q) = S_{\mathrm{N}}(q)$. Such a situation pertains only to rigid chain-like aggregates in the absence of an external magnetic field. Typically, we are dealing with an intermediate situation in which the characteristic correlation length of magnetic moments in a cluster covers several sizes of magnetic monomers but does not exceed the cluster size. The existence of magnetic correlations in clusters is reflected in the magnetization curve that effectively corresponds to a larger magnetic size. However, the Langevin approximation does not work and corrections accounting for the interaction must be introduced. The Langevin approximation also encounters difficulty because corrections used for a concentrated MF are based on the mean field approximation relevant for an infinite system. A cluster is finite; therefore, correlations in magnetic moment orientations in the periphery and center are different. Another complicating factor is the particle polydispersity.

A more sophisticated analysis of the cluster structure based on the SANS data taking magnetic scattering in differently deuterated solvents into account was undertaken

with the use of nonpolarized [36, 45] and polarized (in a magnetic field) [37, 117, 139–143] neutrons. Basic simplifications with respect to magnetic correlations were used; that is, the magnetic moments of the particles were regarded either as totally independent ($S_M(q) = 1$) or as totally correlated ($S_N(q) = S_M(q)$). The latter simplification is based on the assumption that the magnetic moment orientations in a saturation field are fully correlated inside a cluster, similarly to those in a bulk ferromagnet. However, the applicability of this approximation in the case of strongly interacting particles (paramagnetic and polydisperse at the same time) in a cluster is not obvious because the fluctuation region (correlation length) with respect to the field direction is determined by the dipole–dipole interaction that does not involve the whole of the cluster. Moreover, the external magnetic field for the particles interacting by the dipole–dipole mechanism diminishes their reciprocal influence; therefore, the former simplification for the saturation field appears more acceptable. Nevertheless, it is nearly impossible to eliminate the dipole–dipole interaction effect even at rather high fields, as we show in Section 5.

Detection and identification of the cluster structure by the SANS technique are important components of the MF analysis. We emphasize once again that SANS is used to study unmodified bulk samples, meaning that clusters discovered by this method are not artifacts of the pre-experiment treatment of the samples. The authors of Ref. [144] tried to follow up the kinetics of structural changes in MF clusters subjected to a magnetic field. They showed that the characteristic time of structural changes is of the order of several minutes. However, the intensity of the neutron source used in these experiments (a stationary 10 MW reactor) was insufficient to obtain a statistically significant scattering curve in a wide range of q values within the specified time. For all that, the analysis of mean scattering intensity allowed them to reach a number of interesting conclusions about cluster growth dynamics upon switching the magnetic field on and off. The effect of an alternating magnetic field applied to an MF upon polarized neutron scattering was investigated in Refs [145–147]. This stroboscopic approach was used for the analysis of magnetic ordering in aggregated particles of a concentrated Co-containing MF. Magnetic relaxation times in these experiments were hundreds of milliseconds.

The analysis of scattering on chain-like aggregates formed in an MF under the effect of a magnetic field is as difficult (and thus far unresolved) a problem as the structure factor analysis in a magnetized MF. The basic difficulty arises from the coincidence between anisotropies of the interaction potential in the magnetized MF and of the extended aggregates being formed. The corresponding components of scattering can be separated in so-called shearing experiments [148–151]. The application of a magnetic field at an angle to the MF flow direction allows detecting the formation of extended aggregates. However, their quantitative analysis encounters difficulties.

An important issue in magnetic fluid research is the estimation of the MF stability after dilution. The equilibrium distribution of stabilizing agents between the particle surfaces and the solvent is used in both steric (Fig. 3b) and electrostatic (Fig. 3c) stabilizations. A high (thousands of times) degree of dilution of practically optimal compositions ($\varphi_m \sim 0.1-20\%$) may disturb this distribution and cause surfactant desorption, leading to the deterioration of the MF stability and manifesting itself as a sharp increase in cluster formation and phase splitting. Under these conditions, low particle concentrations and the shift of cluster sizes and phase inhomogeneities into the submicron range precludes the efficient use of SANS for the detection and analysis of the respective inhomogeneities. In this case, dynamic light scattering [39, 40] and optical methods [32] are mainly used.

By the SANS technique, not only the aforementioned clusters but also more complicated helical structures [116], agglomerates of magnetic particles and surfactants [37, 117, 140–143], and ordered pseudocrystalline structures induced by an external magnetic field [102, 152–155] can be detected in MFs. The pseudocrystal structures form when the interaction between the particles is strengthened by using strongly magnetic materials (pure Co, Ni, and Fe instead of their oxides) or increasing the particle size. In these cases, linear aggregation is accompanied by chain growth in width and manifestations of the bulk structure exhibiting a pseudocrystalline ordering.

Currently, it is difficult to propose a reliable classification of MF clusters and correlate their formation with MF preparation procedures. In many cases, cluster formation is specifically related to the mode of stabilization, and SANS serves as a diagnostic tool ensuring a reliable detection of clusters and providing information about their internal structure. Consistent investigations into the processes of cluster formation and growth in MFs require the synthesis of model MFs with a rigorously defined primary structure (especially important for aqueous systems) similar to that of polar and nonpolar organic MFs containing isolated particles.

5. Magnetic fluids in an external magnetic field

Application of a magnetic field to an MF in SANS experiments renders magnetic scattering anisotropic with respect to the radial angle φ in the plane of the detector (coinciding to a high degree of precision with the plane of the vector $\mathbf{q}$). Saturation magnetization of low-concentration ($\varphi_m \sim 1\%$) and purely superparamegnetic MFs makes magnetic scattering fully anisotropic, whereas nuclear scattering remains isotropic [156, 157],

$$I(q, \varphi) \sim \langle F_N^2(q) \rangle + \langle F_M^2(q) \rangle \sin^2 \varphi \,, \tag{47}$$

where angular brackets denote averaging over the size distribution function. The analysis of two-dimensional experimental scattering maps taking the $\sin^2 \varphi$ anisotropy into account allows separating the contributions of nuclear and magnetic scatterings. If the magnetic field fails to introduce important structural changes into the MF, then the sum of the separated contributions of the form $\langle F_N^2(q) \rangle + 2/3 \langle F_M^2(q) \rangle$ must give the same scattering curve as in the absence of the field. This procedure for separation of nuclear and magnetic scattering components was successfully used in investigations of classical inorganic MFs (magnetite/OA/benzene) [88, 158]. The analysis of an anisotropic two-dimensional picture of SANS was used in earlier investigations of aggregated aqueous MFs [159–161].

Additional equations for anisotropic scattering in a magnetic field can be derived in the case of a neutron beam polarization (Fig. 17). In the foreign literature, a similar method is referred to as small-angle neutron scattering with

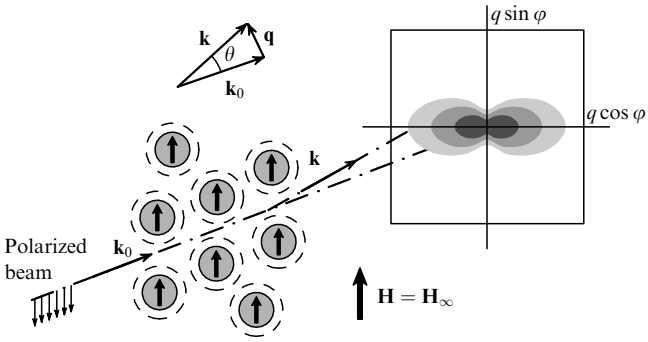

Figure 17. Principal diagram of a SANS experiment with polarized neutrons for an MF in a saturation magnetic field. The magnetic moments of all particles are oriented parallel to the field.

polarization (SANSAPOL) [175]. The first experiments using this approach are described in [162]. A special device (polarizer) orients the neutron magnetic moments of the incident beam in one direction colinear with the magnetic field **H** in the sample. Another device, a spin flipper, regulates neutron spin orientation with respect to **H**. Two relative orientations of the neutron spin, 'along the field' and 'against the field,' correspond to two different two-dimensional scattering intensities:

$$I^+(q,\varphi) \sim \langle F_{\mathrm{N}}^2(q)\rangle + \left(\langle F_{\mathrm{M}}^2(q)\rangle - 2P\langle F_{\mathrm{N}}(q)F_{\mathrm{M}}(q)\rangle\right)\sin^2\varphi\,, \tag{48a}$$

$$I^-(q,\varphi) \sim \langle F_{\mathrm{N}}^2(q)\rangle + \left(\langle F_{\mathrm{M}}^2(q)\rangle + 2P\varepsilon\langle F_{\mathrm{N}}(q)F_{\mathrm{M}}(q)\rangle\right)\sin^2\varphi\,, \tag{48b}$$

where P is the degree of beam polarization and ε is the spin-flipper efficiency. Unlike (47), expressions (48) contain the cross term $\langle F_{\mathrm{N}}(q)F_{\mathrm{M}}(q)\rangle$ with the nuclear and magnetic scattering amplitudes. Unfortunately, polydispersity does not permit using it as effectively as in the case of monodisperse particles, where the $F_{\mathrm{N}}(q)/F_{\mathrm{M}}(q)$ ratio is obtained directly from (48). Nevertheless, expressions (48) are more exact in the context of statistics collection. The simplest way to separate isotropic and anisotropic scattering components in (48) under experimental conditions is radial averaging of the intensity in the vicinity of the angles $\varphi = 0$ and $\pi/2$ in the detector plane corresponding to the directions along and against the field **H**. Such averaging leads to the set of four equations

$$I^+(q,0) = I_{\parallel}^+(q) = \langle F_{\mathrm{N}}^2(q)\rangle\,, \tag{49a}$$

$$I^+\left(q,\frac{\pi}{2}\right) = I_{\perp}^+(q) = \langle F_{\mathrm{N}}^2(q)\rangle + \langle F_{\mathrm{M}}^2(q)\rangle - 2P\langle F_{\mathrm{N}}(q)F_{\mathrm{M}}(q)\rangle\,, \tag{49b}$$

$$I^-(q,0) = I_{\parallel}^-(q) = \langle F_{\mathrm{N}}^2(q)\rangle\,, \tag{49c}$$

$$I^-\left(q,\frac{\pi}{2}\right) = I_{\perp}^-(q) = \langle F_{\mathrm{N}}^2(q)\rangle + \langle F_{\mathrm{M}}^2(q)\rangle + 2P\varepsilon\langle F_{\mathrm{N}}(q)F_{\mathrm{M}}(q)\rangle \tag{49d}$$

for the functions $\langle F_{\mathrm{N}}^2(q)\rangle$, $\langle F_{\mathrm{M}}^2(q)\rangle$, and $\langle F_{\mathrm{N}}(q)F_{\mathrm{M}}(q)\rangle$ to be found from experimental data. Averaging (48) over the entire φ angle is needed to verify an anisotropy like $\sin^2\varphi$. In this case, $\sin^2\varphi$ in (48) is substituted by its mean value $1/2$:

$$\langle I^+(q,\varphi)\rangle_\varphi = I^+(q) = \langle F_{\mathrm{N}}^2(q)\rangle + \frac{1}{2}\langle F_{\mathrm{M}}^2(q)\rangle - P\langle F_{\mathrm{N}}(q)F_{\mathrm{M}}(q)\rangle\,, \tag{50a}$$

$$\langle I^-(q,\varphi)\rangle_\varphi = I^-(q) = \langle F_{\mathrm{N}}^2(q)\rangle + \frac{1}{2}\langle F_{\mathrm{M}}^2(q)\rangle + P\varepsilon\langle F_{\mathrm{N}}(q)F_{\mathrm{M}}(q)\rangle\,. \tag{50b}$$

The function $\langle F_{\mathrm{N}}(q)F_{\mathrm{M}}(q)\rangle$ derived from (50) is compared with the analogous function derived from (49).

The analysis of the small-angle scattering of polarized neutrons was used to study inorganic MFs with single stabilization [26, 31, 163] for which relevant data on nonpolarized neutron scattering were presented above. Figure 18 shows two-dimensional scattering intensities for two MFs ($\varphi_{\mathrm{m}} \approx 1\%$) on a deuterated base (99% D-cyclohexane) and two polarization states of the neutron beam. The scattering components separated according to (49) are shown in Fig. 19. The 'nuclear' form factor is well described by the 'sphere-shell' model (see fitting results in the caption to Fig. 19), which suggests that the particle positions in the solution are independent. At the same time, the magnetic component is indicative of correlations between the magnetic moments of the particles. Indeed, Fig. 19 shows that magnetic scattering data are very much different from the results of the 'noninteracting polydisperse spheres' model (see typical curves of this model in Figs 11–13) and the corresponding magnetic correlation length is greater than the characteristic size of magnetic nanoparticles. This last property is demonstrated in Fig. 19 by comparing Guinier approximations (10).

We believe that the observed effect is related to the influence of the dipole–dipole interaction on the mutual orientation of magnetic moments, even in MFs with a relatively low concentration of nanoparticles ($\varphi_{\mathrm{m}} \approx 1\%$) subjected to a strong magnetic field. Particle polydispersity is an essential factor in this interaction, which significantly complicates the picture of magnetic correlations in MFs.

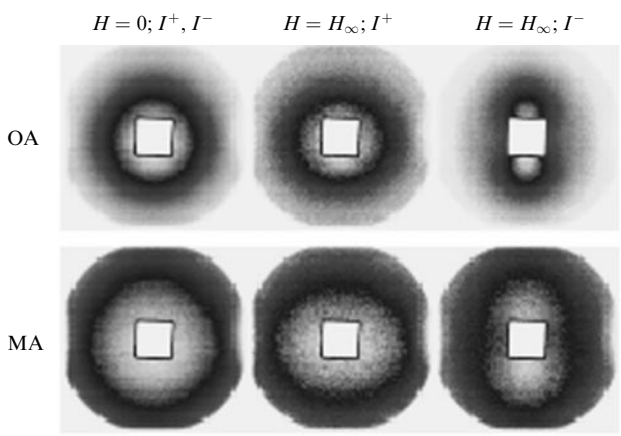

Figure 18. Experimental two-dimensional scattering intensities (GKSS) in various polarization states of incident neutrons for two MFs (magnetite stabilization in D-cyclohexane with OA and MA), $\varphi_{\mathrm{m}} \sim 1\%$ and $H = 2.5$ T. The light square in the center of the detector is an imprint of the beam absorber. Dimples on the edges are marks left by the magnetic system.

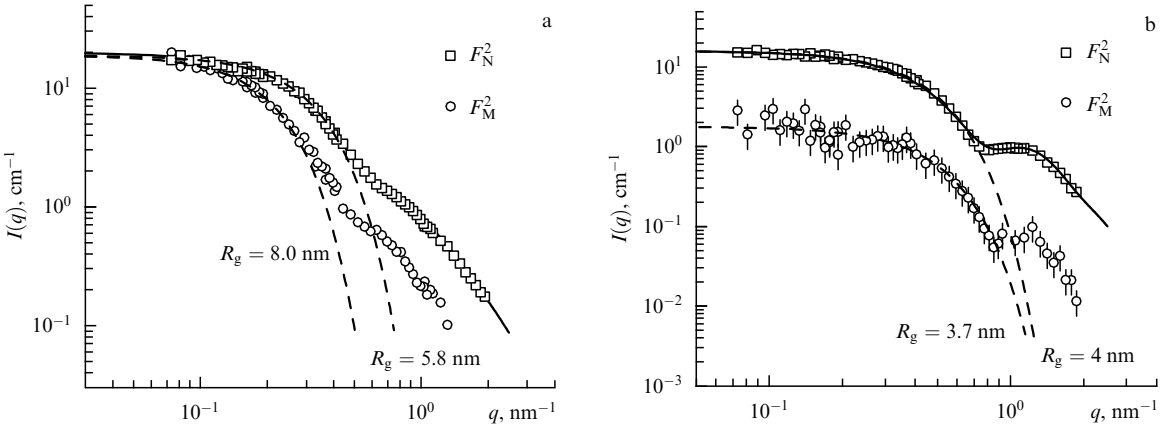

Figure 19. Separated nuclear and magnetic components of neutron scattering (from the polarized neutron scattering data presented in Fig. 18) for D-cyclohexane-based MFs containing (a) OA- and (b) MA-coated magnetite. Solid curves are the fitting by the 'sphere-shell' model taking account of polydispersity (42). Results of fitting: OA sample — $R_0 = 3.4$ nm, $S = 0.38$, $h = 1.38$ nm; MA sample — $R_0 = 2.3$ nm, $S = 0.28$, $h = 1.35$ nm. Dashed curves are Guinier approximation (10) with the observed gyration radii indicated.

As shown in Ref. [88], several forms of such correlations can be arbitrarily distinguished depending on the relative size of the interacting particles as their concentration is increased. A decrease in the concentration to below 1% results in a weakening of magnetic correlations, but the accuracy of determining magnetic scattering curves for large q worsens substantially due to poor statistics, and the background effect on the estimates of integral parameters of the scattering curves acquires importance.

An interesting feature of magnetic correlations is the sum $\langle F_N^2(q)\rangle + 2/3\langle F_M^2(q)\rangle$, which frequently and with good accuracy coincides with the scattering curve measured in the absence of a magnetic field; in other words, correlations observed in the absence of the field persist after it is switched on. Thus far, the sole possibility of explaining this effect is to attribute it to the strong correlation along the orientation of magnetic moments that is responsible for the formation of chain-like aggregates at high MF concentrations. Our data point to the existence of an anisotropic short-range order in MFs with respect to the orientation of the magnetic moments of the particles, even in the absence of direct contact between them. This short-range order is significantly different from that in the particle disposition, as is demonstrated by comparing the effective structure factors in Figs 13a and 15.

The following conclusion is valid as regards the structure of the MF considered: stabilization by the substitution of saturated linear acids (LA, MA, PA, SA) for a classical surfactant (oleic acid) changes the radial distribution function $D_n(R)$ for the dispersed particles as a result of a different organization of the adsorbed molecules on the surface of the magnetic material [31, 34]. In the presence of saturated acids, only part of the magnetic nanoparticles produced in the precipitation reaction is dispersed into the fluid; these particles have a smaller mean size and polydispersity than those in the presence of OA. In view of the good miscibility of OA and saturated acids in solutions, it has been proposed that their mixtures be used to stabilize and regulate the size of MF particles [164]. The nuclear scattering curve obtained with the use of polarized neutrons for a mixture of MA and OA is compared in Fig. 20 with analogous curves for samples stabilized by OA and MA. The function $D_n(R)$ thus obtained confirms the suggestion of size modulation depending on the saturated acid content in the stabilizing mixture. A more detailed analysis in [165] indicated that MA, unlike LA, readily mixes with OA on the magnetite surface, making it possible to change the characteristic size of dispersed magnetite nanoparticles with good accuracy (5%) in the range 5–8 nm and enabling its use to regulate the viscosity and the magnetoviscous effect in an MF under practical conditions. Thus, separation of magnetic scattering into nuclear and magnetic components by the SANSPOL method can be effectively used to obtain purely nuclear scattering curves despite the difficulties inherent in the magnetic scattering analysis.

A similar analysis of SANSPOL scattering was extensively used in studying different types of MFs, including cobalt nanoparticles in a variety of media [37, 139–141, 166, 167], iron nanoparticles in decalin [117], barium hexaferrite particles in dodecane [142], and magnetite nanoparticles with double stabilization [143]. As mentioned above, all these studies revealed an important contribution to scattering from different aggregates present in the MF. An additional

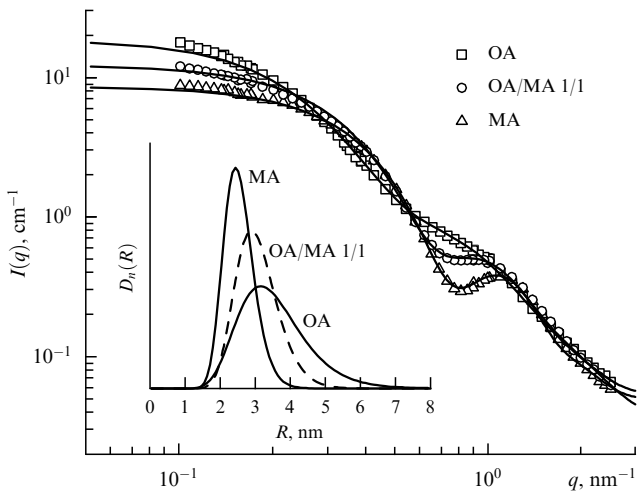

Figure 20. Change in the nuclear scattering curve (GKSS) in the case of magnetite stabilization in D-cyclohexane by adding an MA/OA mixture. The label OA/MA 1/1 indicates the mass ratio of acids in the mixture. The inset shows the functions $D_n(R)$ obtained by direct curve fitting within the 'sphere-shell' model.

fitting of the nuclear scattering component was performed with regard for different contrasts and structure factors (the local polydisperse approximation). It considerably complicated the data interpretation and decreased the informative value of the method due to additional free parameters introduced into the model that are responsible for the structure of aggregates. A procedure for the analysis of the difference curve $I^{+}(q,\varphi) - I^{-}(q,\varphi)$ intended to enhance the reliability of the interpretation is proposed in Ref. [139]. The presence of strong aggregation in the examples being discussed essentially distinguishes the studied systems from MFs shown in Figs 18–20, where SANSPOL is applied to classical MFs whose particles are certainly isolated. We note that the use of different approaches in the SANS framework allowed reliably describing the structure of such MFs, as is shown in Figs 7–9, 11–13, and 18–20.

Using the field dependence of scattering,

$$I^{-,+}(q,\varphi) \sim \Big\{ \left[F_{\mathrm{M}}^2(q)L^2(x) \pm 2F_{\mathrm{M}}(q)F_{\mathrm{N}}(q)L(x)\right] \sin^2\varphi + F_{\mathrm{N}}^2(q) \Big\} S_{\mathrm{N}}(q,\varphi) + F_{\mathrm{M}}^2(q)\left[\frac{2L(x)}{x} - \left(L^2(x) - 1 + \frac{3L(x)}{x}\right)\sin^2\varphi\right], \quad (51)$$

was proposed in order to obtain additional information about the system [168]; here, $L(x) = \coth(x) - 1/x$ is the Langevin function of the variable $x = \mu_0 \mu V H/(k_{\mathrm{B}}T)$. Expression (51) is written for a monodisperse case. Also, it is supposed that at sufficiently strong 'nuclear' (atomic) correlations (corresponding to the structure factor $S_{\mathrm{N}}(q,\varphi)$, which can be anisotropic in the general case) the system preserves its purely superparamagnetic behavior as regards fluctuations of the particle magnetic moments. Expression (51) therefore gives rise to new equations relating nuclear and magnetic scattering components at different H values. This method was called the magnetic contrast variation [168].

We also note the special possibility of estimating the degree of interference between nuclear and magnetic scattering in terms of the optical theorem [169]. The appropriate direct analysis of straight beam broadening was performed for two neutron polarization states in an aqueous MF with double stabilization [170, 171].

Far less frequently used is the so-called complete polarization analysis in which changes in the spin state after scattering are additionally considered (using a polarization analyzer). In this way, four types of intensity for different neutron spin combinations before and after scattering ($I^{++}, I^{+-}, I^{-+}, I^{--}$) are detected instead of two measured by the SANSPOL method. The corresponding system of equations [118] permits separating nuclear and magnetic scatterings without sample magnetization. However, the strong background effect and the large exposure time hamper using this method in practical contexts. Examples of its application are described in Refs [118, 156, 171–175]. A simplified scheme of the analysis of neutron depolarization when passing through the sample can be segregated from this approach; it permits obtaining information on magnetic correlations in the system [110, 161, 167].

Reflectometry using polarized neutron scattering is complementary to the SANS technique. To begin with, it allows determining the distribution of nuclear and magnetic SLD along the normal to either the MF–substrate or the air–MF interface. The analysis of diffuse scattering and grazing incidence small-angle neutron scattering (GISANS) provides data on the distribution of inhomogeneities into and over the surface (lateral correlations) of interfaces. For example, the structure at the MF–silicon crystal interface for aqueous MFs with double magnetite stabilization was determined in Refs [177, 178]. Ordering of MF particles into layered structures at such interfaces in an external magnetic field was discovered in [179]. It was also shown in [178] that the method is sensitive to inhomogeneities at the free MF surface that form in an external magnetic field. The MF surface was additionally analyzed [180] using GISAXS.

Finally, an analysis of the MF dynamic properties by the SANS method was performed with the use of the spin echo technique [181–185], which yielded diffusion coefficients of MF nanoparticles under different conditions and magnetic flow distribution in the bulk and at MF interfaces.

6. Conclusion

Small-angle neutron scattering is extensively used in structural studies of the main types of magnetic nanofluids (1–100 nm). The parallel development of contrast variation techniques (generalization of the basic function approach) and SANSPOL methods has provided a tool for the elucidation of the structure of many MFs and thereby has greatly promoted the understanding of the physical nature of various phenomena in these systems. The analysis of the SANS structure factor ensures effective comparison of particle–particle interactions in MFs, in addition to the determination of the properties of individual MF particles (the size distribution function, the SLD in surfactant magnetic core and shell, the effective surfactant layer thickness, the degree of solvent penetration into the surfactant layer, the character of the magnetic core surface, and so on).

It has been shown in this review that the effective structure factor can be used to identify the type of interaction and predict the behavior of MFs in an external magnetic field as regards magnetorheologic properties, phase separation, and so on. In the case of strong screening of magnetic interactions (e.g., in double stabilization of magnetite at its content about 5% by volume in alcohols), it is possible to qualitatively describe the effective structure factor as an additional method for obtaining information on the structure of MF particles (thickness and degree of overlapping of the surfactant double layer). Cluster formation in MFs is essentially reflected in SANS curves. The analysis of the clusters suggests their complicated (many-level) structure. Branched fractal clusters not infrequently form in MFs along with chain-like (linear) aggregates and may change under changing the temperature and the applied external fields.

An important feature of the results described in this review is the presence of nuclear and magnetic constituents of neutron scattering in SANS experiments, which permits simultaneously obtaining information about atomic and magnetic structures, thus allowing their discrimination and independent interpretation. Owing to this advantage, the characteristics of the particle structure and interparticle interaction in highly stable MFs have been successfully used to explain the macroscopic properties of MFs. Moreover, the SANS method gives the opportunity to directly verify the general theory of dipole–dipole liquids at the microstructure level.

We have discussed the use of structural data obtained by different methods in complementary studies. This very important issue, common to the sciences investigating nanosystems, requires a separate consideration. Its complexity arises first and foremost from the fact that nanosystems are actually colloidal (and therefore nonequilibrium) systems, and the description of their properties in terms of equilibrium thermodynamics is only approximate, to one extent or another. Specifically, an interpretation of the results obtained by scattering techniques is complicated by nonequilibrium particle aggregation (e.g., residual aggregation during dispersion), which does not change the character of scattering curves but causes a shift in the structural parameter values. Due to this, parameters measured by scattering methods in colloidal systems give some idea of their stability. Their use for the precise estimation of certain characteristics, e.g., nonaggregative particle size, requires a separate consideration for each type of system.

Generally speaking, SANS, as a component of comprehensive structural investigations involving a variety of methods (magnetometry, electron microscopy, synchrotron radiation scattering, and so on), provides the structural information for understanding the mechanisms of MF stabilization that has been used to synthesize new highly stable and concentrated MFs with important properties based on organic and inorganic solvents. Specifically, it proved possible to stabilize high-concentration MFs on nonpolar organic bases with saturated monocarboxylic acids. The different stabilization efficiency compared with that of a classical stabilizer (unsaturated oleic acid) can be attributed to the different structural organization of these surfactant molecules at the surface of magnetic particles. Moreover, interactions between free surfactant molecules in the solution during synthesis make an important contribution to their stabilizing potency.

The recent progress in the synthesis of highly stable and concentrated aqueous MFs is the most important and difficult task in the chemistry of these materials. Such MFs look very promising for future technological and biomedical applications. The SANS technique is equally important for basic structural studies and the diagnostics of model or industrial MFs. The high penetrating capacity of neutrons allows diagnosing commercial specimens. Structural characteristics obtained by the SANS method are extensively used to improve the procedures of MF synthesis and property control.

Further development of SANS for MF investigations requires an improvement in the correlation between quantitative estimates and theoretical predictions for particle–particle interaction potentials under different conditions (including the effects of external magnetic fields). This implies a revision of the theory of polydisperse dipole liquids that, up to now, has been based on the monodisperse approximation. Structural investigations show that polydispersity may play an important role in MF stabilization. It manifests itself in magnetorheologic suspensions of magnetic microparticles and is used to redisperse them. Elucidation of this role with reference to MFs with magnetic nanoparticles is of great interest for structural studies, including those with the application of SANS.

Experimental data illustrating the application of SANS and other approaches in this review were obtained by the authors jointly with several research groups from European institutions, including neutron centers, including the Joint Institute for Nuclear Research (JINR); Russian Research Center 'Kurchatov Institute' (RRC KI); the Center of Fundamental and Advanced Technical Research, Romanian Academy of Sciences, Timisoara Branch, Romania (CFATR); the Budapest Neutron Centre, Hungary (BNC); Forschungszentrum Geesthacht, Germany (GKSS); the Institute of Experimental Physics, Slovak Academy of Sciences, Košice, Slovakia (IEP SAS); and Taras Shevchenko Kiev National University, Ukraine (KNU). The authors are grateful to L Vekas (CFATR), L Rosta (BNC), R Willumeit, A Schreyer, V M Garamus (GKSS), L A Bulavin (KNU), P Kopcansky (IEP SAS), M Balasoiu (JINR), A V Feoktystov, V I Petrenko (JINR, KNU), A V Porokhova (Lomonosov Moscow State University), Ya V Zubavichus, and A A Veligzhanin (RRC KI) for the enlightening discussions and assistance in the treatment of experimental MF data obtained by SANS and other methods. Most of them were obtained using MF samples synthesized by D Bica (1952–2008) (CFATR).

The work was supported by the RFBR (Helmholtz–Russia Joint Research Groups, JINR-HRJRG-016, 2007–2010), the Federal Agency for Science and Innovations (Rosnauka) (state contracts No. 02.434.11.2033, No 02.442.11.7375 under the Federal Target Program "Research and Developments in Priority Areas of Science and Technology for 2002–2006" and No. 02.445.11.7003 under the Program for Support of Leading Scientific Schools in Russia). Certain experiments were carried out in the framework of JINR–Hungary and JINR–Romania cooperation programs.

References

1. Rosensweig R E *Ferrohydrodynamics* (Cambridge: Cambridge Univ. Press, 1985)
2. Shliomis M I *Usp. Fiz. Nauk* **112** 427 (1974) [*Sov. Phys. Usp.* **17** 153 (1974)]
3. Odenbach S (Ed.) *Ferrofluids: Magnetically Controllable Fluids and their Applications* (Lecture Notes in Physics, Vol. 594) (Berlin: Springer-Verlag, 2002) p. 233
4. Vekas L, Avdeev M V, Bica D "Magnetic nanofluids: synthesis and structure", in *NanoScience in Biomedicine* (Ed. D Shi) (Berlin: Springer-Verlag, 2009) Ch. 25, p. 650
5. García-Palacios J L "On the statics and dynamics of magnetoanisotropic nanoparticles", in *Advances in Chemical Physics* Vol. 112 (Eds I Prigogine, S A Rice) (New York: Wiley, 2000)
6. Gogosov V V, Simonovskii A Ya, Shaposhnikova G A *Tr. Mat. Inst. Akad. Nauk SSSR* **140–149** 186 (1989)
7. Huke B, Lücke M *Rep. Prog. Phys.* **67** 1731 (2004)
8. Proc. of the 10th Intern. Conf. on Magnetic Fluids, *J. Magn. Magn. Mater.* **289** (2005)
9. Sun S et al. *Science* **287** 1989 (2000)
10. Weller D et al. *IEEE Trans. Magn.* **36** 10 (2000)
11. Zeng H et al. *Nature* **420** 395 (2002)
12. Mornet S et al. *J. Mater. Chem.* **14** 2161 (2004)
13. Wuang S C et al. *Adv. Funct. Mater.* **16** 1723 (2006)
14. Duguet E et al. *Nanomedicine* **1** 157 (2006)
15. Fortin J-P et al. *Am. Chem. Soc.* **129** 2628 (2007)
16. Häfeli U, Schütt W (Eds) *Proc. of the 6th Intern. Conf. on the Scientific and Clinical Applications of Magnetic Carriers — SCAMC-06, Australia, 2006*; *J. Magn. Magn. Mater.* **311** (1) (2007)
17. Häfeli U, Zborowski M (Eds) *Proc. of the 7th Intern. Conf. on the Scientific and Clinical Applications of Magnetic Carriers, Canada, 2008*; *J. Magn. Magn. Mater.* **321** (10) (2009)
18. Avdeev M V et al. *Langmuir* **26** 8503 (2010)
19. Izyumov Yu A *Usp. Fiz. Nauk* **131** 387 (1980) [*Sov. Phys. Usp.* **23** 356 (1980)]

20. Ostanevich Yu M, Serdyuk I N *Usp. Fiz. Nauk* **137** 85 (1982) [*Sov. Phys. Usp.* **25** 323 (1982)]
21. Aksenov V L *Usp. Fiz. Nauk* **161** 179 (1991) [*Sov. Phys. Usp.* **34** 729 (1991)]
22. Aksenov V L, Balagurov A M *Usp. Fiz. Nauk* **166** 955 (1996) [*Phys. Usp.* **39** 897 (1996)]
23. Ozerov R P *Usp. Fiz. Nauk* **167** 541 (1997) [*Phys. Usp.* **40** 517 (1997)]
24. Aksenov V L *Usp. Fiz. Nauk* **172** 701 (2002) [*Phys. Usp.* **45** 645 (2002)]
25. Aksenov V L, Balagurov A M, Pomyakushin V Yu *Usp. Fiz. Nauk* **173** 883 (2003) [*Phys. Usp.* **46** 856 (2003)]
26. Avdeev M V *Usp. Fiz. Nauk* **177** 1139 (2007) [*Phys. Usp.* **50** 1083 (2007)]
27. Aksenov V L *Usp. Fiz. Nauk* **179** 434 (2009) [*Phys. Usp.* **52** 406 (2009)]
28. Lebedev V T et al. *J. Magn. Magn. Mater.* **201** 136 (1999)
29. Bica D et al. *Prog. Colloid Polym. Sci.* **125** 1 (2004)
30. Avdeev M V et al. *J. Colloid Interface Sci.* **295** 100 (2006)
31. Avdeev M V et al. *J. Magn. Magn. Mater.* **311** 6 (2007)
32. Bica D et al. *J. Magn. Magn. Mater.* **311** 17 (2007)
33. Balasoiu M, Avdeev M V, Aksenov V L *Kristallogr.* **52** 528 (2007) [*Crystallogr. Rep.* **52** 505 (2007)]
34. Avdeev M V et al. *J. Colloid Interface Sci.* **334** 37 (2009)
35. Bica D *Romanian Rep. Phys.* **47** 265 (1995)
36. Shen L, Laibinis P E, Hatton T A *Langmuir* **15** 447 (1999)
37. Wiedenmann A, Hoell A, Kammel M *J. Magn. Magn. Mater.* **252** 83 (2002)
38. Vékás L, Bica D, Avdeev M V *China Particuology* **5** 43 (2007)
39. Hajdú A et al. *Prog. Colloid Polym. Sci.* **135** 29 (2008)
40. Tombácz E et al. *J. Phys. Condens. Matter* **20** 204103 (2008)
41. Massart R et al. *J. Magn. Magn. Mater.* **149** 1 (1995)
42. Fauconnier N et al. *Prog. Colloid Polym. Sci.* **100** 212 (1996)
43. Dubois E et al. *Langmuir* **16** 5617 (2000)
44. Gazeau F et al. *Phys. Rev. E* **65** 031403 (2002)
45. Moeser G D et al. *Langmuir* **20** 5223 (2004)
46. Tomašovičová N et al. *Meas. Sci. Rev. Sect. 2* **6** 32 (2006)
47. Sondjaja R, Hatton T A, Tam M K C *J. Magn. Magn. Mater.* **321** 2393 (2009)
48. Porai-Koshits E A *Usp. Fiz. Nauk* **39** 573 (1949)
49. Svergun D I, Feigin L A *Rentgenovskoe i Neitronnoe Malouglovoe Rasseyanie* (Structure Analysis by Small-Angle X-Ray and Neutron Scattering) (Moscow: Nauka, 1986) [Translated into English (New York: Plenum Press, 1987)]
50. Brumberger H (Ed.) *Modern Aspects of Small-Angle Scattering* (Dordrecht: Kluwer Acad. Publ., 1995)
51. Pedersen J S *Adv. Colloid Inter. Sci.* **70** 171 (1997)
52. Freltoft T, Kjems J K, Sinha S K *Phys. Rev. B* **33** 269 (1986)
53. Martin J E, Hurd A J *J. Appl. Cryst.* **20** 61 (1987)
54. Teixeira J *J. Appl. Cryst.* **21** 781 (1988)
55. Schmidt P W, in *Modern Aspects of Small-Angle Scattering* (Ed. H Brumberger) (Dordrecht: Kluwer Acad. Publ., 1995) p. 1
56. Beaucage G *J. Appl. Cryst.* **29** 134 (1996)
57. Mandelbrot B B *The Fractal Geometry of Nature* (San Francisco: W.H. Freeman, 1982)
58. Avnir D (Ed.) *The Fractal Approach to Heterogeneous Chemistry* (Chichester: John Wiley and Sons, 1989)
59. Bale H D, Schmidt P W *Phys. Rev. Lett.* **53** 596 (1984)
60. Kjems J K, Schofield P, in *Scaling Phenomena in Disordered Systems* (NATO ASI Series B: Physics, Eds R Pynn, A Skeltorp) (New York: Plenum Press, 1985) p. 141
61. Kaiser R, Miskolczy G *J. Appl. Phys.* **41** 1064 (1970)
62. Berkowitz A E et al. *Phys. Rev. Lett.* **34** 594 (1975)
63. Mollard P, Germi P, Rousset A *Physica B + C* **86–88** 1393 (1977)
64. Han D H et al. *J. Appl. Phys.* **76** 6591 (1994)
65. Haneda K, Morrish A H *J. Appl. Phys.* **63** 4258 (1988)
66. Tronc E et al. *Hyperfine Interact.* **112** 97 (1998)
67. Lin D et al. *J. Magn. Magn. Mater.* **145** 343 (1995)
68. Kodama R H et al. *Phys. Rev. Lett.* **77** 394 (1996)
69. Hendriksen P V, Linderoth S, Lindgård P-A *Phys. Rev. B* **48** 7259 (1993)
70. Aquino R et al. *Phys. Rev. B* **72** 184435 (2005)
71. Shendruk T N et al. *Nanotechnology* **18** 455704 (2007)
72. Stuhrmann H B, in *Small Angle X-Ray Scattering* (Eds O Glatter, O Kratky) (London: Academic Press, 1982)
73. Stuhrmann H B, in *Modern Aspects of Small-Angle Scattering* (Ed. H Brumberger) (Dordrecht: Kluwer Acad. Publ., 1995) p. 221
74. Perkins S J *Biochem. J.* **254** 313 (1988)
75. Avdeev M V *J. Appl. Cryst.* **40** 56 (2007)
76. Cebula D J, Charles S W, Popplewell J *J. Magn. Magn. Mater.* **39** 67 (1983)
77. Grabcev B et al. *Magnit. Gidrodinamika* **30** 156 (1994) [*Magnetohydrodynamics* **30** 130 (1994)]
78. Grabcev B et al. *J. Magn. Magn. Mater.* **201** 140 (1999)
79. Feoktystov A V et al. *Poverkhnost. Rentgen. Sinkhrotron. Neitron. Issled.* (1) 3 (2009) [*J. Surf. Invest. X-Ray, Synchr., Neutron Tech.* **3** 1 (2009)]
80. Feoktystov A V et al. *Solid State Phenomena* **152–153** 186 (2009)
81. Whitten A E, Cai S, Trewhella J *J. Appl. Cryst.* **41** 222 (2008)
82. Feoktystov A V et al. *Ukr. J. Phys.* **54** 348 (2009)
83. Avdeev M V et al. *J. Appl. Cryst.* **43** 959 (2010)
84. Balasoiu M et al. J. *Magn. Magn. Mater.* **300** e225 (2006)
85. Feoktystov A V et al. *Ukr. J. Phys.* **54** 266 (2009)
86. Avdeev M V et al. *J. Appl. Cryst.* **42** 1009 (2009)
87. Avdeev M et al. *J. Magn. Magn. Mater.* **252** 86 (2002)
88. Avdeev M V et al. *J. Magn. Magn. Mater.* **270** 371 (2004)
89. Török Gy et al. *Romanian Rep. Phys.* **58** 293 (2006)
90. Shen L et al. *Langmuir* **17** 288 (2001)
91. Balasoiu M et al. *Magnetohydrodynamics* **40** 359 (2004)
92. Avdeev M V et al. *Solid State Phenomena* **152–153** 182 (2009)
93. Eberbeck D, Bläsing J *J. Appl. Cryst.* **32** 273 (1999)
94. Török Gy et al. *J. Magn. Magn. Mater.* **300** e221 (2006)
95. Petrenko V I et al. *Poverkhnost. Rentgen. Sinkhrotron. Neitron. Issled.* (2) 92 (2009) [*J. Surf. Invest. X-Ray, Synchr., Neutron Tech.* **3** 161 (2009)]
96. Petrenko V I et al. *Fiz. Tverd. Tela* **52** 913 (2010) [*Phys. Solid State* **52** 974 (2010)]
97. Aswal V K et al. *Pramana* **63** 285 (2004)
98. Mehta R V et al. *J. Magn. Magn. Mater.* **149** 47 (1995)
99. Upadhyay T et al. *Phys. Rev. B* **55** 5585 (1997)
100. Bläsing J, Strassburger G, Eberbeck D *Phys. Status Solidi A* **146** 595 (1994)
101. Itri R et al. *Eur. Phys. J. E* **4** 201 (2001)
102. Klokkenburg M et al. *Phys. Rev. E* **75** 051408 (2007)
103. Lemaire B J et al. *Eur. Phys. J. E* **13** 291 (2004)
104. Wagner J, Autenrieth T, Hempelmann R *J. Magn. Magn. Mater.* **252** 4 (2002)
105. Narsinga Rao G et al. *Phys. Rev. E* **72** 031408 (2005)
106. Vorobiev A et al. *J. Appl. Cryst.* **41** 831 (2008)
107. Porokhova A V et al. *Izv. Vyssh. Uchebn. Zaved. Fizika* **53** (3/2) 176 (2010)
108. Rasa M *Eur. Phys. J. E* **2** 265 (2000)
109. Socoliuc V, Bica D, Vekas L *J. Colloid Interface Sci.* **264** 141 (2003)
110. Balasoiu M, Aksenov V L *J. Optoelectron. Adv. Mater.* **10** 3322 (2008)
111. Balasoiu M et al. *Magnetohydrodynamics* **44** 61 (2008)
112. Balasoiu M et al. *Pis'ma Zh. Eksp. Teor. Fiz.* **88** 243 (2008) [*JETP Lett.* **88** 210 (2008)]
113. Pelster R, Spanoudaki A, Kruse T *J. Phys. D* **37** 307 (2004)
114. Kruse T et al. *Phys. Rev. B* **67** 094206 (2003)
115. Butter K, Philipse A P, Vroege G J *J. Magn. Magn. Mater.* **252** 1 (2002)
116. Neto C, Bonini M, Baglioni P *Colloid Surf. A* **269** 96 (2005)
117. Butter K et al. *J. Appl. Cryst.* **37** 847 (2004)
118. Gazeau F et al. *J. Phys. Condens. Matter* **15** S1305 (2003)
119. Vékás L et al. *Prog. Colloid Polym. Sci.* **117** 104 (2001)
120. Cousin F, Cabuil V *Prog. Colloid Polym. Sci.* **115** 77 (2000)
121. Dubois E et al. *J. Chem. Phys.* **111** 7147 (1999)
122. Boué F et al. *J. Magn. Magn. Mater.* **122** 78 (1993)
123. Mériguet G et al. *J. Magn. Magn. Mater.* **289** 39 (2005)
124. Hayes C F *J. Colloid Interface Sci.* **52** 239 (1975)
125. Peterson E A, Krueger D A *J. Colloid Interface Sci.* **62** 24 (1977)
126. Ivanov A O *Kolloid. Zh.* **57** 347 (1995)
127. Vrij A *J. Chem. Phys.* **71** 3267 (1979)
128. Frenkel D et al. *J. Chem. Phys.* **84** 4625 (1986)
129. Mériguet G et al. *J. Phys. Chem. B* **110** 4378 (2006)

130. Mériguet G et al. *J. Phys. Condens. Matter* **18** S2685 (2006)
131. Davies P et al. *J. Phys. D* **19** 469 (1986)
132. Camp P J, Patey G N *Phys. Rev. E* **62** 5403 (2000)
133. Huang J P, Wang Z W, Holm C *Phys. Rev. E* **71** 061203 (2005)
134. Michels A, Weissmüller J *Eur. Phys. J. B* **26** 57 (2002)
135. Cerdà J J et al. *Phys. Rev. E* **81** 011501 (2010)
136. Balasoiu M et al. *Mater. Sci. Forum.* **373–376** 457 (2001)
137. Aksenov V L et al. *Poverkhnost. Rentg. Sinkhrotr. Neitr. Issled.* (7) 11 (2002)
138. Lecommandoux S et al. *J. Magn. Magn. Mater.* **300** 71 (2006)
139. Heinemann A, Wiedenmann A *J. Appl. Cryst.* **36** 845 (2003)
140. Kammel M, Wiedenmann A, Hoell A *J. Magn. Magn. Mater.* **252** 89 (2002)
141. Kammel M et al. *Physica B* **385** 457 (2006)
142. Hoell A et al. *J. Magn. Magn. Mater.* **252** 92 (2002)
143. Kammel M, Hoell A, Wiedenmann A *Script. Mater.* **44** 2341 (2001)
144. Aksenov V L et al. *J. Magn. Magn. Mater.* **258** 452 (2003)
145. Wiedenmann A et al. *Physica B* **385–386** 453 (2006)
146. Wiedenmann A et al. *Phys. Rev. B* **77** 184417 (2008)
147. Keiderling U, Wiedenmann A *J. Appl. Cryst.* **40** s62 (2007)
148. Odenbach S, Gilly H, Lindner P *J. Magn. Magn. Mater.* **201** 353 (1999)
149. Pop L M et al. *Appl. Organomet. Chem.* **18** 523 (2004)
150. Pop L M et al. *J. Magn. Magn. Mater.* **289** 303 (2005)
151. Pop L M, Odenbach S *J. Phys. Condens. Matter* **18** S2785 (2006)
152. Wiedenmann A et al. *Phys. Rev. E* **68** 031203 (2003)
153. Wiedenmann A, Kammel M, Hoell A *J. Magn. Magn. Mater.* **272–276** 1487 (2004)
154. Wiedenmann A, Heinemann A *J. Magn. Magn. Mater.* **289** 58 (2005)
155. Heinemann A, Wiedenmann A *J. Magn. Magn. Mater.* **289** 149 (2005)
156. Pynn R, Hayter J B, Charles S W *Phys. Rev. Lett.* **51** 710 (1983)
157. Wiedenmann A *J. Appl. Cryst.* **33** 428 (2000)
158. Aksenov V et al. *Appl. Phys. A* **74** 943 (2002)
159. Rosman R, Janssen J J M, Rekveldt M Th *J. Magn. Magn. Mater.* **85** 97 (1990)
160. Rosman R, Janssen J J M, Rekveldt M Th *J. Appl. Phys.* **67** 3072 (1990)
161. Rekveldt M Th "Small angle neutron scattering and neutron depolarization by magnetic small particles", in *Magnetic Properties of Fine Particles* (Eds J L Dormann, D Fiorani) (Amsterdam: North-Holland, 1992)
162. Itoh S et al. *J. Magn. Magn. Mater.* **103** 126 (1992)
163. Balasoiu M et al. *Romanian Rep. Phys.* **58** 305 (2006)
164. Vékás L et al., GeNF Annual Report 2006 (Geestchaht: GKSS, 2007)
165. Avdeev M V et al., in *7th Intern. Conf. on the Scientific and Clinical Applications of Magnetic Carrier, Vancouver, Canada, 2008*, Book of Abstracts
166. Bonini M, Wiedenmann A, Baglioni P *J. Phys. Chem. B* **108** 14901 (2004)
167. Bonini M, Wiedenmann A, Baglioni P *Physica A* **339** 86 (2004)
168. Heinemann A, Wiedenmann A, Kammel M *Physica B* **350** E207 (2004)
169. Toperverg B et al. *Physica B* **267–268** 203 (1999)
170. Vorobiev A et al. *Physica B* **276–278** 694 (2000)
171. Hayter J, Pynn R *Phys. Rev. Lett.* **49** 1103 (1982)
172. Aksel'rod L A et al. *Zh. Eksp. Teor. Fiz.* **91** 531 (1986) [*Sov. Phys. JETP* **64** 312 (1986)]
173. Török Gy, Lebedev V T, Orlova D N *Magnetohydrodynamics* **38** 277 (2002)
174. Lebedev V T et al. *Physica B* **234–236** 525 (1997)
175. Lebedev V T et al. *Magnetohydrodynamics* **38** 271 (2002)
176. Zabenkin V N et al. *Appl. Phys. A* **74** (Suppl. 1) s710 (2002)
177. Toperverg B et al. *Physica B* **283** 203 (2000)
178. Vorobiev A et al. *Physica B* **297** 194 (2001)
179. Vorobiev A et al. *Phys. Rev. Lett.* **93** 267203 (2004)
180. Vorobiev A et al. *Phys. Rev. E* **79** 031403 (2009)
181. Lebedev V T et al. *J. Magn. Magn. Mater.* **122** 83 (1993)
182. Lebedev V T et al. *J. Magn. Magn. Mater.* **201** 80 (1999)
183. Lebedev V T et al. *J. Magn. Magn. Mater.* **201** 133 (1999)
184. Lebedev V T, Török Gy, Toperverg B P *J. Magn. Magn. Mater.* **252** 95 (2002)
185. Achiwa N et al. *Physica B* **335** 104 (2003)